Fall 2017

Energy Storage Management and Simulation for Nano-Grids

Shantu Ghose

ENERGY STORAGE MANAGEMENT AND SIMULATION FOR NANO-GRIDS

by

SHANTU GHOSE

(Under the Direction of Adel El Shahat)

ABSTRACT

Energy storage has been utilized in many forms and applications from a flashlight to the Space Shuttle. There is a worldwide effort to develop battery model with high energy level and power densities for a variety range of applications, including hybrid electric vehicles (HEV) and photovoltaic system (PV). To improve battery technology, understanding the battery modeling is very important. So, modeling the thermal behavior of a battery is a vital consideration before designing an effective thermal management system which will operate safely and prolong the lifespan of an energy storage system. The first part of this work focused on the aging model of lithium-ion battery and a simple thermal model of lithium-ion and lead-acid battery using MATLAB/Simulink. After that, an artificial neural network model (ANN) is developed to predict various characteristics at wide temperature range. In this case, comparisons between the training/testing data outputs and targets validating both models with a regression accuracy of 99.839% and 98.727% respectively for Li-ion and Lead-Acid battery while it is 99.912% for the aging model of Li-ion battery. In the end, this energy storage device is used to interconnect with HOMER. This HOMER project aims at designing a solar-wind hybrid power system for Statesboro, Georgia. The cost analysis is performed utilizing HOMER software based on solar irradiance, wind speed, and residential load profile. The proposed HOMER model, using solar & wind with the grid was more cost efficient as the cost of energy (COE) was found 0.0618$/kWh

where the average residential electricity rate in Statesboro is 0.116$/kWh. As a result of using this model, the total cost is reduced by 46.72% compared to other conventional power systems. In the second part of HOMER simulation, while comparing among three types of storage devices, another minimum COE is found using wind with grid connection. As the wind speed is good enough for Statesboro, Georgia, simulation shows that minimum COE is 0.0499$/kWh, 0.0386$/kWh and 0.0633$/kWh respectively for Li-ion, Lead-acid, and Vanadium.

INDEX WORDS: Storage device, Renewable energy, Battery aging, Thermal modeling, ANN, HOMER, NPC, Cost of energy, Hybrid power system.

ENERGY STORAGE MANAGEMENT AND SIMULATION FOR NANO-GRIDS

by

SHANTU GHOSE

B.S. in Electrical Engineering, Chittagong University of Engineering and Technology, Bangladesh, 2011

M.S., Georgia Southern University, 2017

A Thesis Submitted to the Graduate Faculty of Georgia Southern University in Partial

Fulfillment of the Requirements for the Degree

MASTER OF SCIENCE

STATESBORO, GEORGIA

ENERGY STORAGE MANAGEMENT AND SIMULATION FOR NANO-GRIDS

by

SHANTU GHOSE

Major Professor: Adel El Shahat

Committee: Mohammad Ahad

Rami Haddad

Electronic Version Approved:
December 2017

DEDICATION

This thesis work is dedicated to my parents.

ACKNOWLEDGEMENTS

First of all, I would like to express my sincere thanks to my research supervisor, Dr. Adel El Shahat, for his invaluable guidance and support throughout my research. Through all the tremendous effort Dr. Shahat spent on me, I improved myself greatly in many aspects, and of which the most important part is the research attitude – never stop challenging myself. All of the training and improvements will definitely benefit me in the future work.

I also thank my parents and all family members and friends for their constant support during my thesis work.

TABLE OF CONTENTS

ACKNOWLEDGEMENTS 3

LIST OF FIGURES 8

LIST OF SYMBOLS 13

CHAPTER 1 14

INTRODUCTION 14

1.1 Background 14

1.2 Energy Storage DC Nano-grid 17

1.2.1 Energy Storage 17

1.2.2 Energy Storage DC Nano-grid 17

1.3 Why Energy Storage 20

1.4 Scope of Battery Aging and Thermal Model 21

1.5 Research Objectives 22

CHAPTER 2 23

LITERATURE REVIEW 23

2.1 Aging Process of Li-ion Battery 23

2.1.1 Aging Model 24

2.2 Thermal Modeling for Lithium-Ion Battery 25

2.2.1 Battery Parameters 26

2.2.2 Circuit Description 28

2.2.3 Simulation Results 28

2.3 Thermal Modeling for Lead-Acid Battery 29

2.3.1 Battery Model 29

2.3.2 Branch Voltage 29

2.3.3 Terminal Resistance and Main Branch Resistance 1 & 2 29

2.3.4 Main Branch Capacitance 1 30

2.3.5 Parasitic Branch Current 30

2.3.6 State of Charge and Depth of Charge 30

2.3.7 Simulation Results 31

CHAPTER 3 33

METHODOLOGY 33

3.1 ANN-Predictive Thermal Batteries Models 33

3.1.1 Artificial Neural Networks (ANNs) Technique 33

3.2 Designing ANN Models 36

3.2.1 Design with ANN 36

3.2.2 Data Collection 36

3.2.3 Data Processing 37

3.2.4 Building the Network 37

3.2.5 Training the Network 37

3.2.6 Testing the Network 37

3.3 Lithium-Ion Battery ANN Model 37

3.3.1 Li-Ion Battery Aging Model 37

3.3.2 Li-Ion Battery Thermal Model 44

3.3.3 Lead-Acid Battery ANN Model 49

3.4 HOMER Simulation 55

3.4.1 Solar and Wind Availability 55

3.4.2 Data Collection 56

3.5 HOMER Simulation Model 57

3.5.1 Generic Flate Plate PV 58

3.5.2 Wind Turbine 58

3.5.3 Storage Device 58

3.5.4 System Converter 59

3.5.5 Advanced Grid 59

3.5.6 Optimization Outputs 60

3.6 Comparison of Distinct Types of Storage Devices using HOMER 63

3.7 Correlation of Technical Parameters 64

3.7.1 Storage Devices 64

3.7.2 Charging Time 64

3.7.3 Cycle Life 65

3.7.4 Rate Execution 65

3.7.5 Frosty Weather Performance 65

3.7.6 Ecological Impact & Recycling 65

3.7.7 Analysis of Cost 66

3.7.8 Electricity Production & State of Charge (SOC) 67

CHAPTER 4 69

RESULTS 69

4.1 Lithium-Ion Battery 69

4.1.1 Li-Ion Battery Aging Model 69

4.1.2 Li-Ion Battery Thermal Model 73

4.2 Lead-Acid Battery Thermal Model 75

4.3 Output from HOMER 77

4.3.1 Optimization Results 77

CHAPTER 5 81

CONCLUSION 81

5.1 Summary of Present Work 81

5.2 Future Work 82

REFERENCES 83

LIST OF FIGURES

Figure 1: Renewable energy sources (Enclyclopaedia Britannica, n.d.). 15

Figure 2: Renewable electricity generation ((EIA), Annual Energy Outlook 2015, April, 2015) 16

Figure 3: Electricity production from renewable and non-renewable sources (Global Energy Statistical Yearbook, 2017)..... 17

Figure 4: Block diagram of DC microgrid (Konrad, Loria, Miller, & Yamasaki, May 5, 2014). 18

Figure 5: Concept of the electric power system (Cvetkovic I. , July,2010) 19

Figure 6: A feasible future home (Salameh & Davis, 2003) (Cvetkovic, et al., 2009) 20

Figure 7: Aging process of Li-ion batteries (Groot, 2014) 23

Figure 8: Electrochemistry-based Model (Leng F. e., Effect of Temperature on the Aging rate of Li-ion Battery Operating above Room Temperature, 2015)..... 24

Figure 9: Thermal model of Li-ion battery (M. & Dessaint, n.d.)..... 26

Figure 10: Simulation results (a) battery voltage (b) battery current (c) SOC and (d) ambient & internal temp of Li-ion battery (M. & Dessaint, n.d.)..... 28

Figure 11: Thermal model of Lead-acid battery (Jackey R. A.)..... 31

Figure 12: Simulation results at 25C (a) load current (b) SOC (c) temperature (d) terminal voltage (e) DOC and (f) heat flow (Jackey R. A.)..... 32

Figure 13: Neuron function (El-Shahat, 2014) 34

Figure 14: Example of a multiple layers feed-forward neural-network (Silva, Spatti, Flauzino, & Liboni, 2016)..... 35

Figure 15: Flow diagram of ANN model..... 36

Figure 16: ANN aging model & design..... 38

Figure 17: Network construction for aging model..... 38

Figure 18: Hidden layer of aging model 39
Figure 19: Output layer of aging model 39
Figure 20: Output layer weights of aging model 39
Figure 21: Hidden layer weights of aging model 40
Figure 22: Training state of aging model 41
Figure 23: Mean square error of aging model 41
Figure 24: Absolute error for aging model 42
Figure 25: Regression factor for training data of aging model 42
Figure 26: Comparison for the testing data of aging model 43
Figure 27: ANN model & design. 44
Figure 28: Network construction 45
Figure 29: Hidden layer 45
Figure 30: Output layer 45
Figure 31: Output layer weights 45
Figure 32: Hidden layer weights 46
Figure 33: Training state 47
Figure 34: Mean square error 47
Figure 35: Regression factor for the training data 48
Figure 36: Comparison for the testing data 48
Figure 37: ANN model & design 49
Figure 38: Network construction 50
Figure 39: Hidden layer 50
Figure 40: Output Layer 50

Figure 41: Output layer weights 51

Figure 42: Hidden layer weights 52

Figure 43: Training state 53

Figure 44: Mean square error 53

Figure 45: Regression factor for the training data 54

Figure 46: Comparison for the ANN model testing data 54

Figure 47: Power curve for 10 kW AC 56

Figure 48: (a) Average-daily-sun-irradiance per month, (b) Average-daily-wind-speed per month 56

Figure 49: (a) Framework arrangement in HOMER (grid connected), (b) Framework arrangement in HOMER (off-grid) 57

Figure 50: Cost curve of Li-ion battery 59

Figure 51: Screenshot of optimized results (grid connected) 61

Figure 52: Screenshot of simulation for finding optimal design (without grid) 61

Figure 53: Snapshot of electricity production & consumption 61

Figure 54: Snapshot of monthly average electricity production 62

Figure 55: Cost curve for (a) 1 kW Li-ion (b) 1 kW Lead-acid (c) Generic Vanadium 64

Figure 56: Cost summary of (a) 1 kW Li-ion [ASM] (b) 1 kW Lead-acid [ASM] (c) Generic Vanadium 67

Figure 57: Monthly electric production for (a) Li-ion (b) Lead-acid (c) Generic Vanadium 67

Figure 58: SOC of (a) Vanadium (100%) (b) Lead-acid (51%) (c) Li-ion (22.5%) 68

Figure 59: Maximum charge storage capacity (Q_m) 69

Figure 60: The aging of m1 of cobalt-oxide electrode 69

Figure 61: The aging of rate constant vs. temperature 70

Figure 62: Total resistance of electrodes resistance and electrode/electrolyte resistance 70

Figure 63: The aging of m2 of graphite electrode 71

Figure 64: The aging of Warburg element resistance 71

Figure 65: The aging of Warburg element capacitance 72

Figure 66: The aging of Warburg RC time constant 72

Figure 67: Comparison between training and output data of aging model 73

Figure 68: Output voltage in volts at different temperature 74

Figure 69: State of Charge (SOC) at different temperature 74

Figure 70: Ambient & Internal temperature in Celsius 74

Figure 71: State of Charge (SOC) at different temperature range 75

Figure 72: Depth of Charge (DOC) at different temperature range 76

Figure 73: Charging/Load current in ampere at different temperature range 76

Figure 74: Internal temperature in Celsius 77

Figure 75: Heat flow in watts at different temperature range 77

Figure 76: Comparison among three different storage devices 79

Figure 77: Screenshot of optimized results (Li-ion/grid connected) 79

Figure 78: Screenshot of optimized results (Li-ion/without grid) 80

Figure 79: Screenshot of optimized results (Lead-acid/grid connected) 80

Figure 80: Screenshot of optimized results (Vanadium/grid connected) 80

LIST OF TABLES

Table 2.1: Battery Parameters (Tremblay, Dessaint, & Dekkiche, 2007)..... 27

Table 3.1: Technical Data for HOMER Model..……...59

Table 3.2: Optimized Analysis for the Cost..…….62

Table 3.3: Cost Analysis for Batteries..…….66

Table 4.1: Optimization Outputs for Different Batteries..…….78

LIST OF SYMBOLS

Symbol	Explanation
E	No-load Voltage (v)
E_o	Battery Constant Voltage (v)
K	Polarization Voltage (v)
Q	Battery Capacity (Ah)
A	Exponential Zone Amplitude (v)
B	Exponential Zone Time Constant Inverse $(Ah)^{-1}$
R	Internal Resistance (Ω)
i	Battery Current (A)
$\int idt$	Actual Battery Charge (Ah)
V_{batt}	Battery Voltage (v)
E_{Full}	Fully Charged Voltage (v)
E_m	Open Circuit Voltage (EMF)
E_{m0}	Open Circuit Voltage at Full Charge
K_E	Constant in volts/ºC
θ	Electrolyte Temperature in ºC
R_o	Resistance (Ω)
R_{oo}	Value of R_o at SOC =1
A_o	Constant
R_1	Main Branch Resistance-1 (Ω)
R_{10}	Constant (Ω)
R_2	Main Branch Resistance-2 (Ω)

R_{20}	Constant (Ω)
A_{21}	Constant
A_{22}	Constant
I_m	Main Branch Current in Amps
I^*	Nominal Battery Current in Amps
C_1	Main Branch Capacitance in Farads
τ_1	Main Branch Constant in Seconds
I_P	Current Loss in Parasitic Branch
V_{PN}	Voltage at Parasitic Branch
G_{P0}	Constant in Seconds
τ_P	Parasitic Branch Time Constant in Seconds
V_{Po}	Constant in Volts
A_P	Constant
θ	Electrolyte Temperature in °C
θ_f	Electrolyte Freezing Temperature in °C
SOC	State of Charge
DOC	Depth of Charge
Q_e	Battery's Charge in Amp-seconds
C	Battery's Capacitance
I_{avg}	Mean Discharge Current in Amps
ρ	Air Density
R	Blade Length
V	Wind Speed

CHAPTER 1

INTRODUCTION

1.1 Background

Energy storage is continuing to play an essential part in power world today. To achieve a secure and sustainable power industry, the first step needs to take is making the electricity grids smarter with the integration of renewable energy resources (RES) (Boroyevich, Cvetkovic, Burgos, & Dong, Intergrid: A Future Electronic Energy Network, Sept. 2013). Renewable energy resources (RES) can capture their energy from on-going natural processes, such as sunlight, wind, tidal energy and geothermal heat flow (Twidell & Weir, 2006). Some of them are infinite while some of them have an only limited amount in nature. Moreover, some of them, for example, solar or wind are available in a natural way to use, but some of them should be formed like coal. Renewable energy sources are always free of carbon. That means it will not create any CO_2 that can cause air pollution. Renewable energy will not run out from nature, and that is why it is called green energy. Renewable energy is a pathway to a sustainable energy future. It can be converted to electricity and later that can be stored or transported to home. We can list some other examples of renewable energy which are present in the immediate environment and can be tapped. These are wave energy, wind energy, solar energy, tidal current energy, biomass, hydro and geothermal energy. Figure 1 shows various types of renewable energy sources which are available in nature.

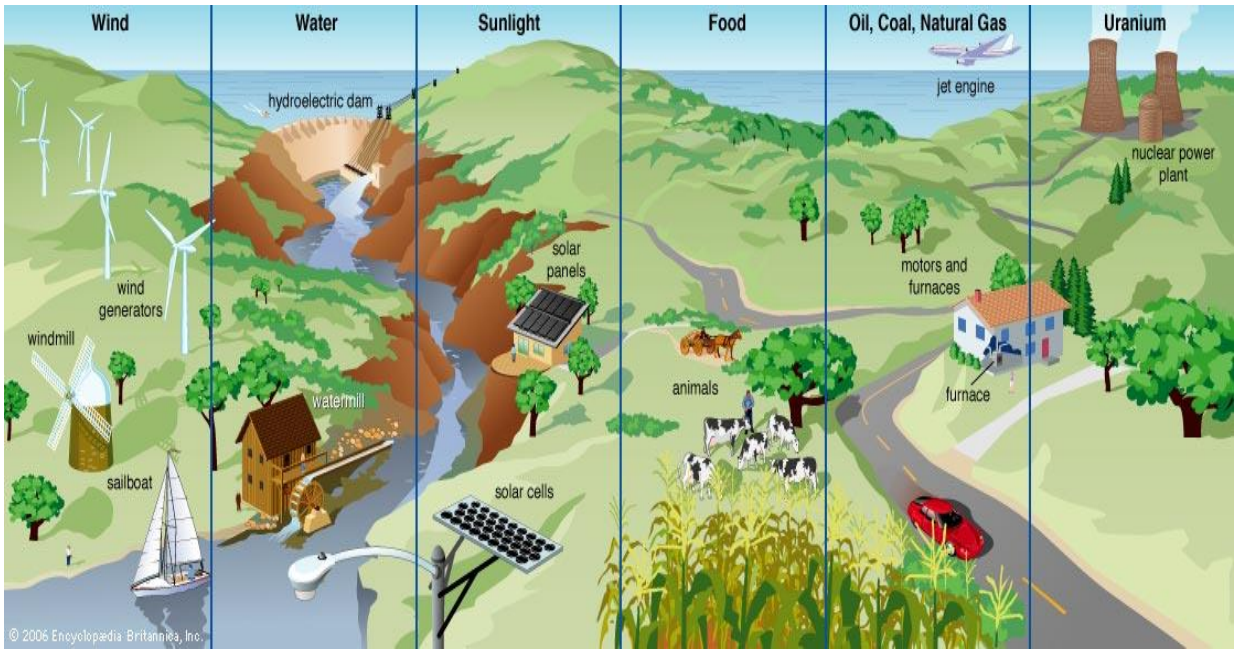

Figure 1: Renewable energy sources (Enclyclopaedia Britannica, n.d.).

According to annual energy report by the U.S. Energy Information Agency (EIA) ((EIA), Annual Energy Outlook, April 2015), renewable energy is expected to grow significantly from 2013 to 2040. From figure 2 it is clear that largest growth will be in the field of solar and wind. In 2013, total non-hydropower renewable generation was nearly equal to hydroelectric generation (Zhang W. , May, 2015). On the other hand, in 2040, non-hydropower will contribute more than sixty percent of total renewable generation. In this case, the total share of renewable generation will increase from 13 percent in 2013 to 18 percent in 2040 (Zhang W. , May, 2015).

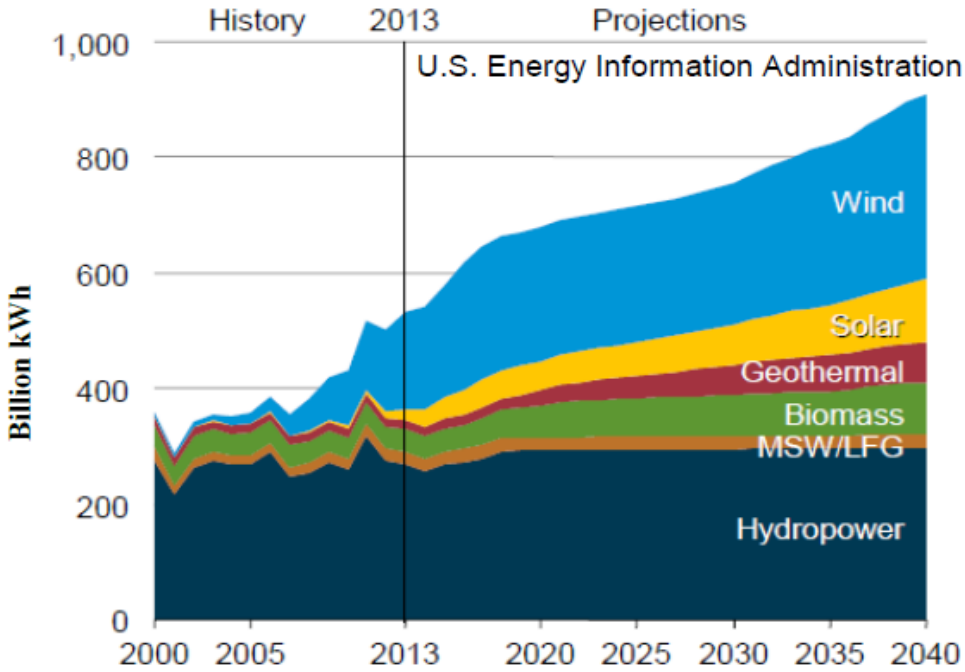

Figure 2: Renewable electricity generation ((EIA), Annual Energy Outlook 2015, April, 2015)

Although, to produce adequate energy from available renewable energy sources is one of the major issues. With the increase of world population and economic growth, we need more energy. Renewable energy is gradually gaining interest in recent research due to the considerations on the depleting nature of non-renewable resources and availability of renewable energy resources. As a result, every nation is looking for a solution for producing energy from renewable energy sources with current technologies. According to the Global Energy Statistical Yearbook 2017 (Global Energy Statistical Yearbook, 2017), figure 3 describes the statistical data of electricity production from renewable energy in different countries of the world. We can see that about 22 percent of total U.S. electricity comes from renewable energy sources (Global Energy Statistical Yearbook, 2017).

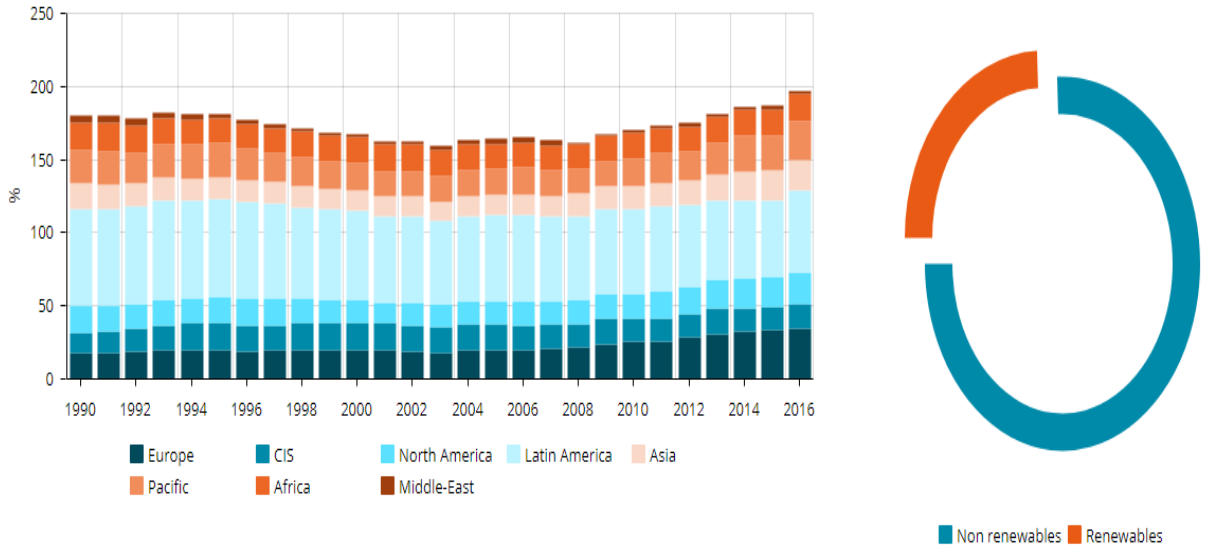

Figure 3: Electricity production from renewable and non-renewable sources (Global Energy Statistical Yearbook, 2017)

1.2 Energy Storage DC Nano-grid

1.2.1 Energy Storage

An energy storage device mainly used for storing electric energy when needed and releasing it when required to operate on next stage. There are various energy storages in mobile small-powered applications such as mobile phone, laptop, etc., and in vehicular applications such as hybrid electric vehicles (HEV) and electric vehicles (EVs). For large-scale energy storages such as pumped hydro storages (PHS) and compressed air energy storages (CAES) have been widely used (Duong, 2013).

1.2.2 Energy Storage DC Nano-grid

Traditionally, for small-scale power applications, Battery Energy Storage System (BESS) is typically used for energy capacity because of its high energy density. On the other side, Flywheel Energy Storage System (FESS) and Ultra-Capacitor (UC) are typically used for fast power

dynamics due to their high-power density. For large-scale power applications, Pumped Hydro Storage (PHS) and Compressed Air Energy Storage (CAES) are used for both energy and power purposes.

In micro-grid and renewable energy plants, when there is need of a medium scale or large-scale energy storage, and PHS and CAES are inaccessible, the only solution is to coordinate small-scale energy storage frameworks together to shape an energy storage DC Nano-grid. To get better efficiency and integration, energy storage nano-grid should be DC rather than AC. Figure 4 gives the initial idea of DC micro-grid.

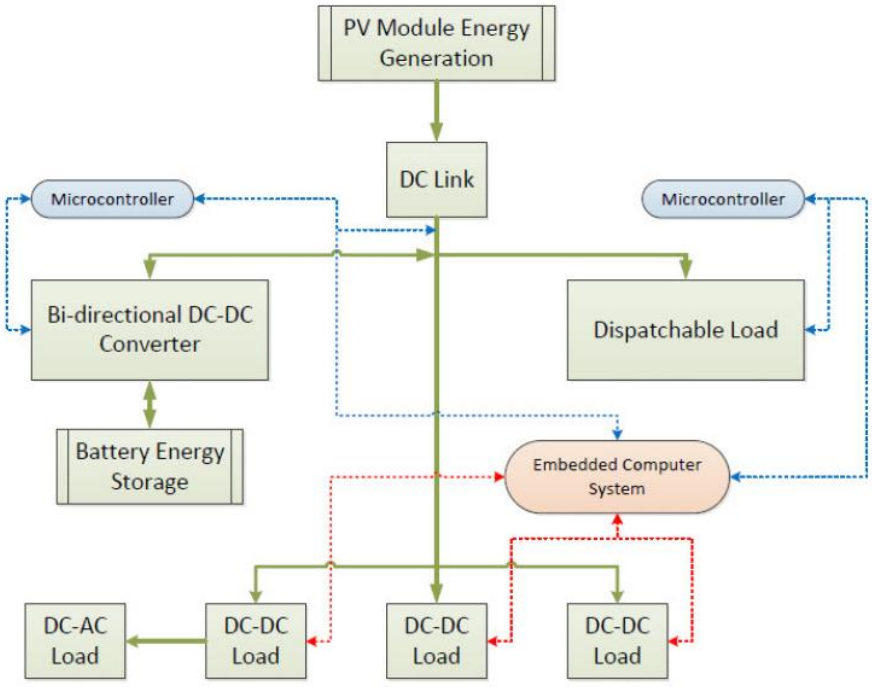

Figure 4: Block diagram of DC microgrid (Konrad, Loria, Miller, & Yamasaki, May 5, 2014)

For micro-grid applications, the energy storage DC Nano-grid can store redundant energy during the normal mode of micro-grid and support the energy to micro-grid during island mode. The energy storage DC Nano-grid also can provide fast power back-up during the transient period of micro-grid from normal mode to island mode or vice versa.

Nano-grids are one kind of micro-grids, which can serve a single building or a single load. Figure 5 describes the modern power system. Here power comes from various types of power plants like nuclear, coal or hydroelectric, etc. using HVDC (high voltage DC) system (Eriksson, Nov 2011) (Wright, Rogers, Manwell, & Ellis, Jun 2002). Nano-grid consists of energy storage with generating units to achieve the maximum output from accessible renewable energy. We can divide micro-grid into AC and DC nano-grids. The residential setup (up to 25 kW) is known as AC nano-grid.

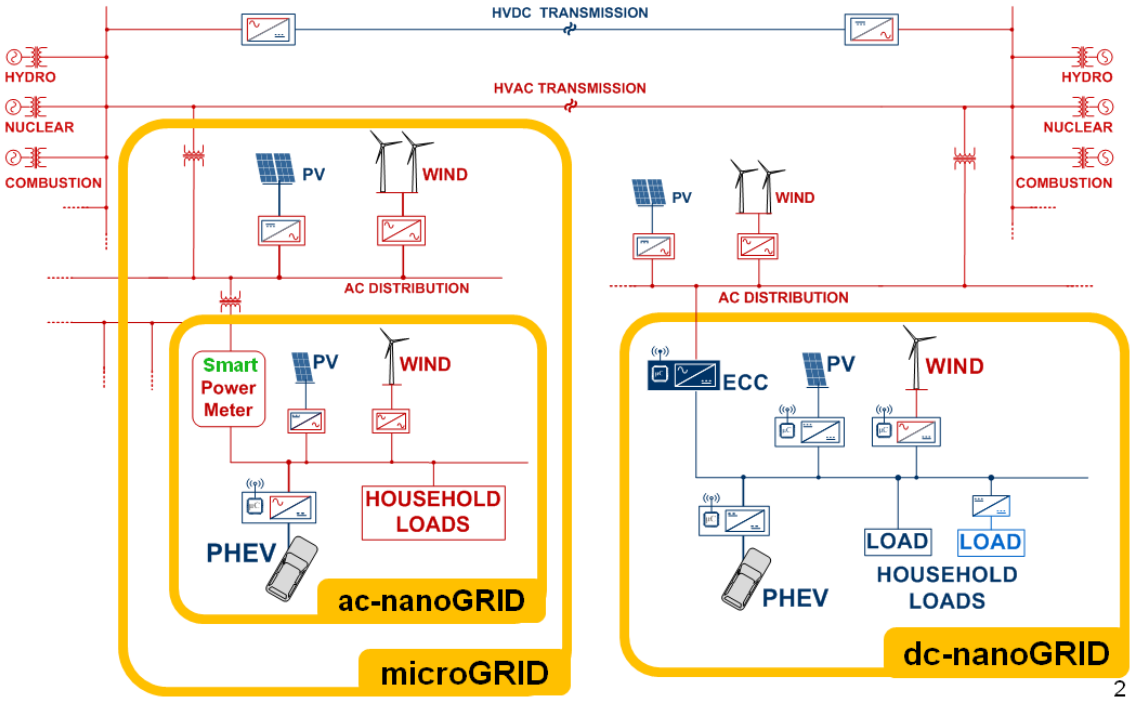

Figure 5: Concept of the electric power system (Cvetkovic I. , July,2010)

AC nano-grid is an integral part of an electric power system which is shown in figure 5. So, a smart future home includes several types of renewable energy sources combined with grid connection. It includes (a) renewable source: solar panels as PV system and wind turbine, (b) energy storage devices: hybrid electric vehicles (HEV) and battery (c) utility grid connection through energy control center (ECC) and (d) loads: home appliances (Salameh & Davis, 2003)

(Cvetkovic, et al., 2009). Figure 6 showing the interconnections and elements of an assortment of home electric energy segments that together include a feasible home with the AC-nanogrid framework.

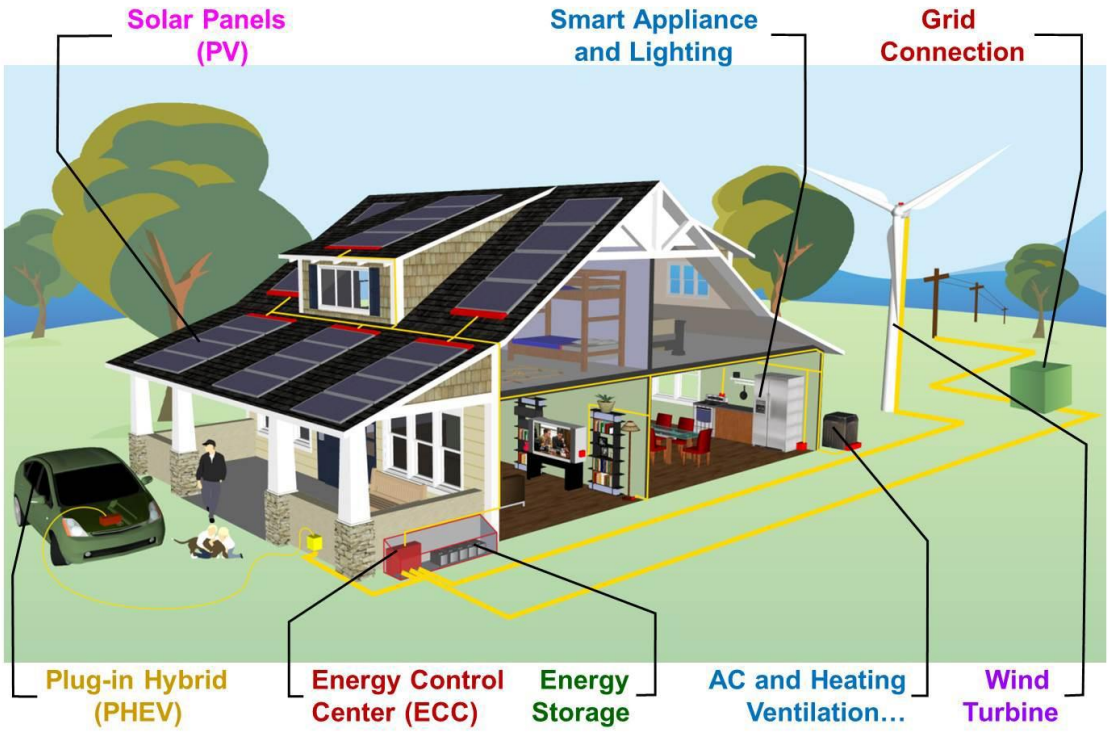

Figure 6: A feasible future home (Salameh & Davis, 2003) (Cvetkovic, et al., 2009)

1.3 Why Energy Storage

We can choose energy storage mainly for three reasons

1. Less carbon energy in future
2. Energy security and reliability
3. Energy price

Low carbon energy future means a vast reduction in the emission of CO_2 from electricity generation, transport and heating systems.

Energy security ensures the ability for energy supply. As oil and gas from the North Sea are declining day by day, experts forecast that within 2020, 50-60 percent oil will be imported while the percentage is more than 70 for gas (Department of Energy and Climate Change, 2010). So, we need energy security policy to fulfill this growing demand. On the other hand, reliability cope with random deviations in supply and demand. A dependable energy network is one in which energy must be given consistently when it is important there must be negligible "loss-of-load" probability.

Energy price is directly related to the variation in supply and demand. It is linked to the economy and effects the price of a traded product. Oil prices exceed hundred dollars for a barrel in 2012 (BP Statistical Review of World Energy., 2012). Energy storage can be a solution of maintaining price stability in the electricity market.

1.4 Scope of Battery Aging and Thermal Model

Noteworthy research efforts are being made to understand and mitigate the degradation of Li-ion batteries upon usage. Battery aging models can be used to optimize the battery usage to achieve robust battery solutions. To design the battery aging model one of the most important factors is temperature. It significantly affects the performance, safety, and cycle lifetime of Lithium-ion batteries (LiB). Although the comprehensive effects of temperature on the aging behavior of Lithium-ion batteries (LiB) have yet to be found (Leng F. e., Effect of Temperature on the Aging rate of Li-Ion Battery Operating above Room Temperature, 2015).

On the other hand, the near future will be more dependent on hybrid electric vehicles (HEV) as they are the most encouraging alternative solution to reduce the greenhouse gases in the car industry. Especially, plug-in HEV and a vehicle-to-grid idea will have a powerful impact in both reductions of greenhouse gases and electricity distribution system (Tremblay, Dessaint, &

Dekkiche, 2007). So, all of these new technologies will depend on battery modeling. As a result, it is very essential to develop accurate battery models. By using ANN (artificial neural network) technique both the battery aging and thermal model can be developed to predict various characteristics at wide temperature range. In this study, ANN models were implemented with an optimal number of layers and neurons, which were trained, simulated and at last verified with 99.912% regression accuracy for the aging model of Li-ion battery while this percentage is 99.839 and 98.727 for the thermal model of Li-ion and Lead-acid battery.

1.5 Research Objectives

This study concentrates on the Li-ion battery aging model and thermal modeling of both Li-ion and lead-acid battery. The goal is to improve the regression accuracy of both aging and thermal model using ANN (Artificial Neural Network). In addition, cost analysis has been done for wind-solar hybrid power system for Statesboro, Georgia. To fulfill these goals, the following procedures were conducted:

- Development of aging model of Li-ion battery and thermal modelling of both lithium-ion and lead-acid battery using ANN.
- Several types of model parameters like maximum charge storage capacity, aging of resistance & capacitance, aging of rate constant, SOC (state of charge), DOC (depth of charge), load current, heat flow etc. are described in the form of 3D figure.
- A study to validate the proposed HOMER model based on actual location-based monthly solar irradiance and wind speed.
- Cost analysis is performed for electricity generation utilizing HOMER.

CHAPTER 2

LITERATURE REVIEW

There has been tremendous research work to the advancement of various existing rechargeable batteries. Among them, lithium-based batteries appear to occupy a prime position in different viewpoints (Kennedy, Patterson, & Camilleri, 2000). In purpose of significant production of HEVs, performance analysis and aging behavior of Li-ion batteries is very important. This chapter addresses a brief description of the existing battery aging process and thermal modeling of lithium-ion and lead-acid batteries.

2.1 Aging Process of Li-ion Battery

The study of the aging process is not an easy task. The most common studied regarding aging mechanism on electrode level made by Vetter (Vetter, et al., March, 2005) is shown in figure 7.

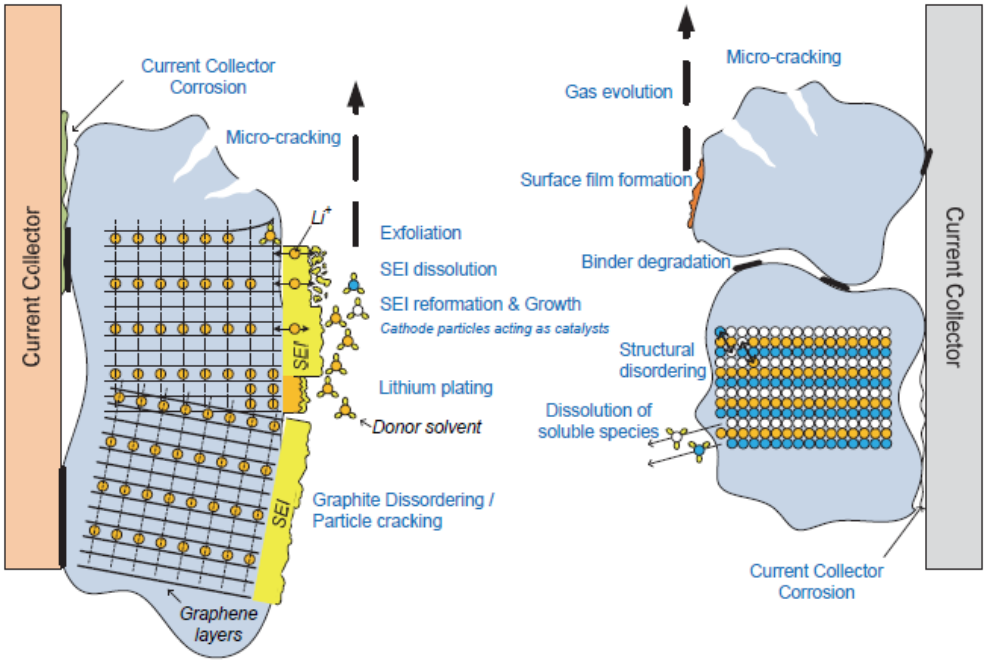

Figure 7: Aging process of Li-ion batteries (Groot, 2014)

Aging mechanism is very much related with operating conditions (Broussely, et al., 2005) and can be categorized into following terms: (a) loss of electrode material (b) loss of cyclable lithium and (c) loss of conductivity in electrodes or electrolyte.

2.1.1 Aging Model

Lots of work has been done in the field of battery modeling. It includes electrochemical models, equivalent circuit based models and impedance based models (Narula, 2014).

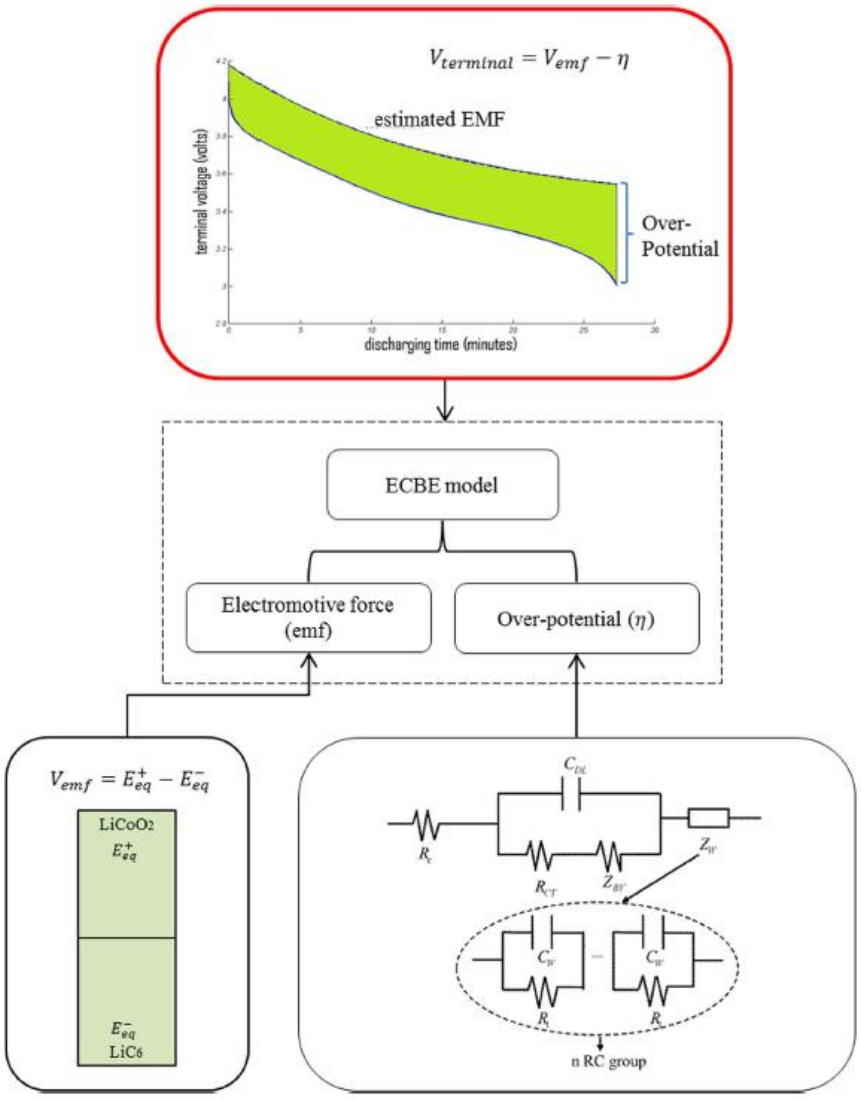

Figure 8: Electrochemistry-based Model (Leng F. e., Effect of Temperature on the Aging rate of Li-ion Battery Operating above Room Temperature, 2015).

ECBE (electrochemistry-based model) is created based on the first principle of electrochemistry and then convert the partial differential equations into circuit model. After that, it is validated by electrochemical impedance spectrometer (EIS) which is the most well-known aging identification tool for various types of LiB (lithium-ion batteries) cells (Leng, Tan, Rachid, & Le, 2014).

Figure 8 represents the most developed ECBE which is used to measure the effects of aging behavior of cycled Li-ion battery within 25°C to 55°C temperature range (Leng F. e., Effect of Temperature on the Aging rate of Li-ion Battery Operating above Room Temperature, 2015). Feng found that due to surface film and phase changes on the LCO (Li-cobalt) electrodes is the main reason to increase in the degradation rate of the maximum charge capacity of the lithium-ion battery (Leng F. e., Effect of Temperature on the Aging rate of Li-ion Battery Operating above Room Temperature, 2015).

From experimental analysis, Feng concluded that degradation rates of Li-ion increases with the increase of temperature which includes maximum charge capacity, charge transfer rate, total resistance, Warburg element resistance, Warburg element capacitance and Warburg RC time constant (Leng F. e., Effect of Temperature on the Aging rate of Li-ion Battery Operating above Room Temperature, 2015).

2.2 Thermal Modeling for Lithium-Ion Battery

A mathematical model of a battery can be defined by a voltage regarding current and state of charge (SOC). This model included a simple voltage source in series with a constant resistance (M. & Dessaint, n.d.).

We can define voltage source by equation (2.1)

$$E = E_o - K\frac{Q}{Q - it} + Aexp\left(-B.\int idt\right) \quad 2.1$$

$$V_{batt} = E - R.i \quad 2.2$$

Where, E = no-load voltage (V), E_o = battery constant voltage (V), K = polarization voltage (V), Q = battery capacity (Ah), $\int idt$ = actual battery charge (Ah), A = exponential zone amplitude (V), B = exponential zone time constant inverse $(Ah)^{-1}$, V_{batt} = battery voltage (V), R = internal resistance (Ω), i = battery current (A).

2.2.1 Battery Parameters

There are three major points which are used to find out model parameters are: charged voltage, end of exponential zone and end of a nominal zone. The exponential part ($Aexp(-B.it)$) is calculated as follows

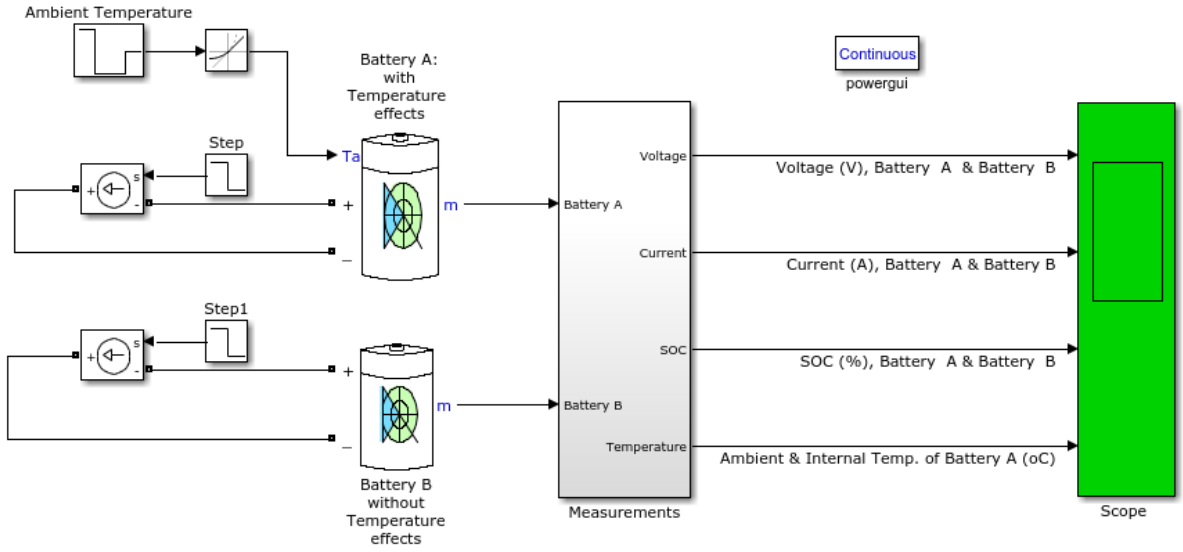

Figure 9: Thermal model of Li-ion battery (M. & Dessaint, n.d.).

A: voltage drop during the exponential zone (V)

$$A = E_{Full} - E_{Exp}$$

$$A = 1.4V - 1.25V = 0.15V \quad (2.3)$$

3 / (B): charge at the end of exponential zone (Ah)

$$BB = \frac{3}{Q_{Exp}} \quad (2.4)$$

$$B = \frac{3}{1.3A.1h} = 2.308(Ah) - 1 \quad (2.5)$$

Equation (2.1) is used to calculate other parameters. Polarization voltage (K) can be found from fully charged voltage (E_{Full}) and end of nominal zone

$$K = \frac{\left(E_{Full} - E_{Nom} + A(\exp(-B.Q_{Nom}) - 1)\right).(Q - Q_{Nom})}{Q_{Nom}}$$

$$K = 0.0125\ (V) \quad (2.6)$$

TABLE 2.1 BATTERY PARAMETERS (Tremblay, Dessaint, & Dekkiche, 2007)

Type Parameters	Lithium-ion 3.6 V 1Ah	Lead-acid 12 V 1.2 Ah
E_o (V)	3.7348	12.6463
R (Ω)	0.09	0.25
K (V)	0.00876	0.33
A (V)	0.468	0.66
B $(Ah)^{-1}$	3.5294	2884.61

Then we can easily calculate voltage constant E_o

$$Eo = E_{Full} + K + Ri - A$$

$$Eo = 1.4 + 0.0125 + 0.0046 * 1.3 - 0.15 = 1.268(V) \quad (2.7)$$

We can use this approach and can be implemented to other types of battery like Lead-acid or Nickel-Cadmium to determine model parameters.

2.2.2 Circuit Description

This model shows the effect of temperature change of a 7.4 V, 5.4 Ah Li-ion battery (LiCoO2). The ambient and internal temperature can be varied during charging and discharging process.

2.2.3 Simulation Results

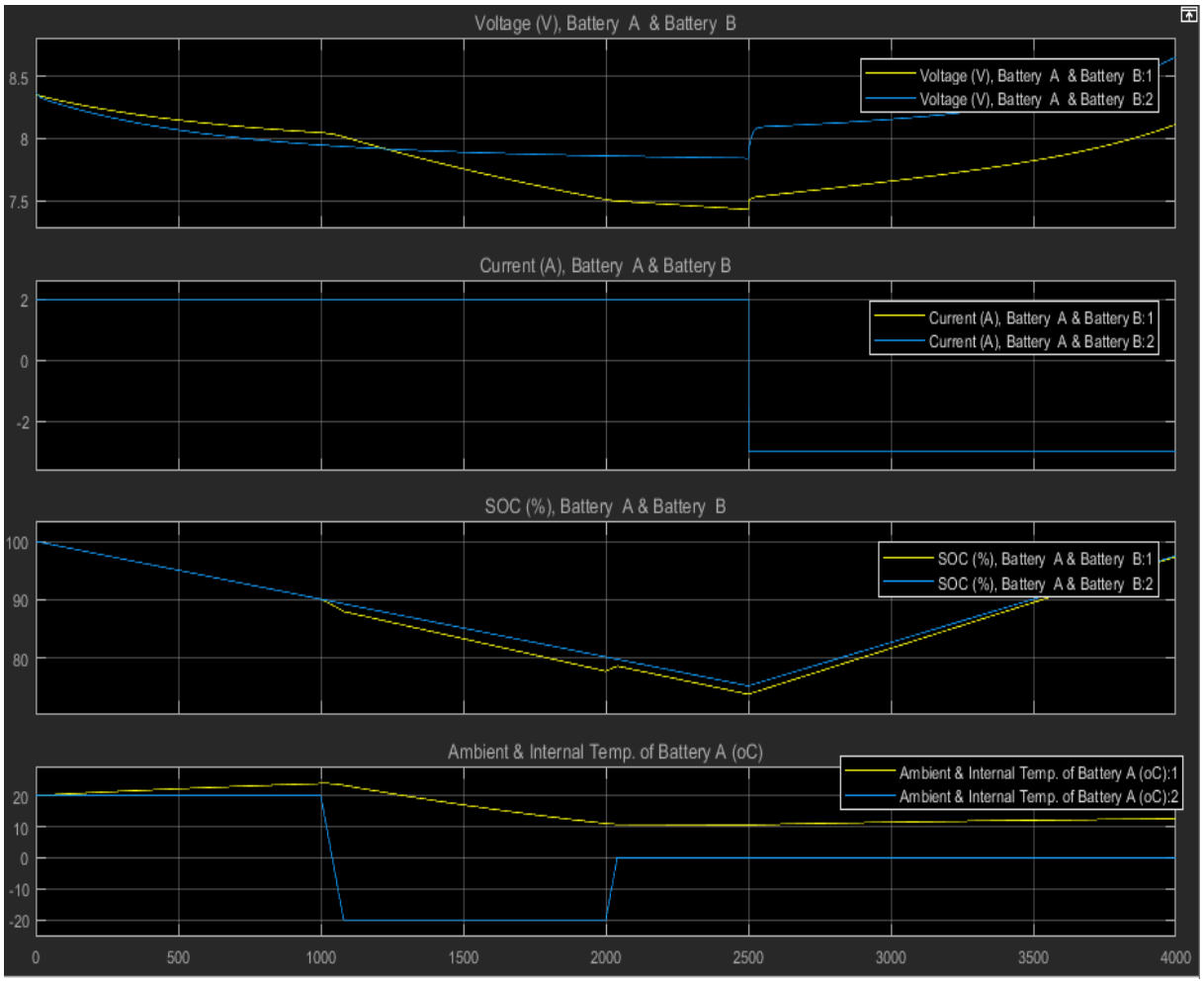

Figure 10: Simulation results (a) battery voltage (b) battery current (c) SOC and (d) ambient & internal temp of Li-ion battery (M. & Dessaint, n.d.).

2.3 Thermal Modeling for Lead-Acid Battery

2.3.1 Battery Model

A physical system of a lead-acid battery consists of three parts: thermal model, a charge with capacity model and an equivalent circuit model (Jackey R. A.). Thermal model works with electrolyte temperature whether the charge and capacity model keep tracks of battery's state of charge (SOC), depth of charge (DOC) and battery's capacity. Battery equivalent circuit acts on battery circuit equations as well as battery current and nonlinear circuit elements.

2.3.2 Branch Voltage

It represents open circuit voltage for one cell. It varies with temperature and state of charge (SOC).

$$E_m = E_{m0} - K_E(273 + \theta)(1 - SOC) \quad 2.8$$

Where E_m= open circuit voltage (EMF) in volts, E_{m0}= open circuit voltage at full charge, K_E= constant in volts/ ^oC, θ= electrolyte temperature in ^oC, SOC= battery state of charge

2.3.3 Terminal Resistance and Main Branch Resistance 1 & 2

Terminal resistance is assumed to be constant and can be varied with SOC.

$$R_o = R_{oo}[1 + A_o(1 - SOC) \quad 2.9$$

Where R_o= resistance in ohms, R_{oo}= value of R_o at SOC =1 in Ohms, A_o= constant.

Main branch resistance 1, varied with DOC (depth of charge). It increases in an exponential way when the battery exhausted during discharge.

$$R_1 = -R_{10} \ln(DOC) \quad 2.10$$

Where R_1= main branch resistance in ohms, R_{10}= constant in ohms, DOC= battery depth of charge

Main branch resistance 2, increases in an exponential way when the battery state of charge increased.

$$R_2 = R_{20}\ \frac{\exp[A_{21}(1-SOC)]}{1+\exp(\frac{A_{22}I_m}{I^*})} \quad 2.11$$

Where R_2= main branch resistance in ohms, R_{20}= constant in ohms, A_{21}, A_{22}= constant, E_m= open circuit voltage in volts, I_m= main branch current in Amps, I^*= nominal battery current in Amps

2.3.4 Main Branch Capacitance 1

$$C_1 = \tau_1/R_1 \quad 2.12$$

Here C_1= main branch capacitance in Farads, τ_1= main branch constant in seconds, R_1 = main branch resistance in ohms

2.3.5 Parasitic Branch Current

$$I_P = V_{PN}G_{P0}\exp(\frac{V_{PN}/(\tau_P S+1)}{V_{Po}} + A_P(1-\frac{\theta}{\theta_f}) \quad 2.13$$

Where I_P= current loss in the parasitic branch, V_{PN} = voltage at the parasitic branch, G_{P0} = constant in seconds, τ_P = parasitic branch time constant in seconds, V_{Po} = constant in volts, A_P = a constant, θ = electrolyte temperature in °C, θ_f = electrolyte freezing temperature in °C

2.3.6 State of Charge and Depth of Charge

$$\mathrm{SOC} = 1 - \frac{\mathrm{Q_e}}{\mathrm{C}(0,\theta)} \quad 2.14$$

$$\mathrm{DOC} = 1 - \frac{\mathrm{Q_e}}{\mathrm{C}(\mathrm{I_{avg}},\theta)} \quad 2.15$$

Here SOC = battery state of charge, DOC = battery depth of charge, Q_e = the battery's charge in Amp-seconds, C = the battery's capacity in Amp-seconds, θ = was electrolyte temperature in °C, I_{avg} = the mean discharge current in Amps

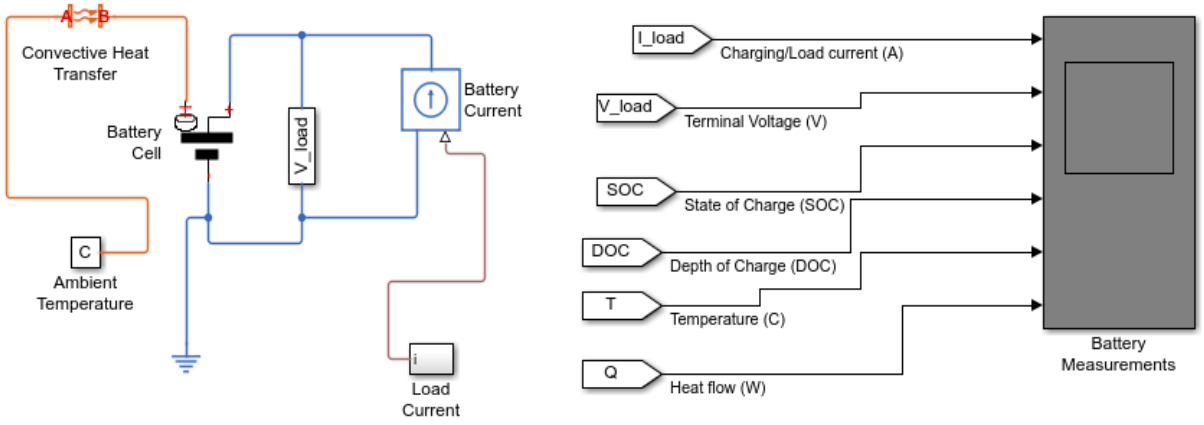

Figure 11: Thermal model of Lead-acid battery (Jackey R. A.).

2.3.7 Simulation Results

In this simulation, at first, the battery is discharged at a constant current of 10A. The battery is then recharged at a constant 10A back to the primary state of charge. Here cooling is primarily using convection, and that heating is mostly from battery internal resistance, R_2.

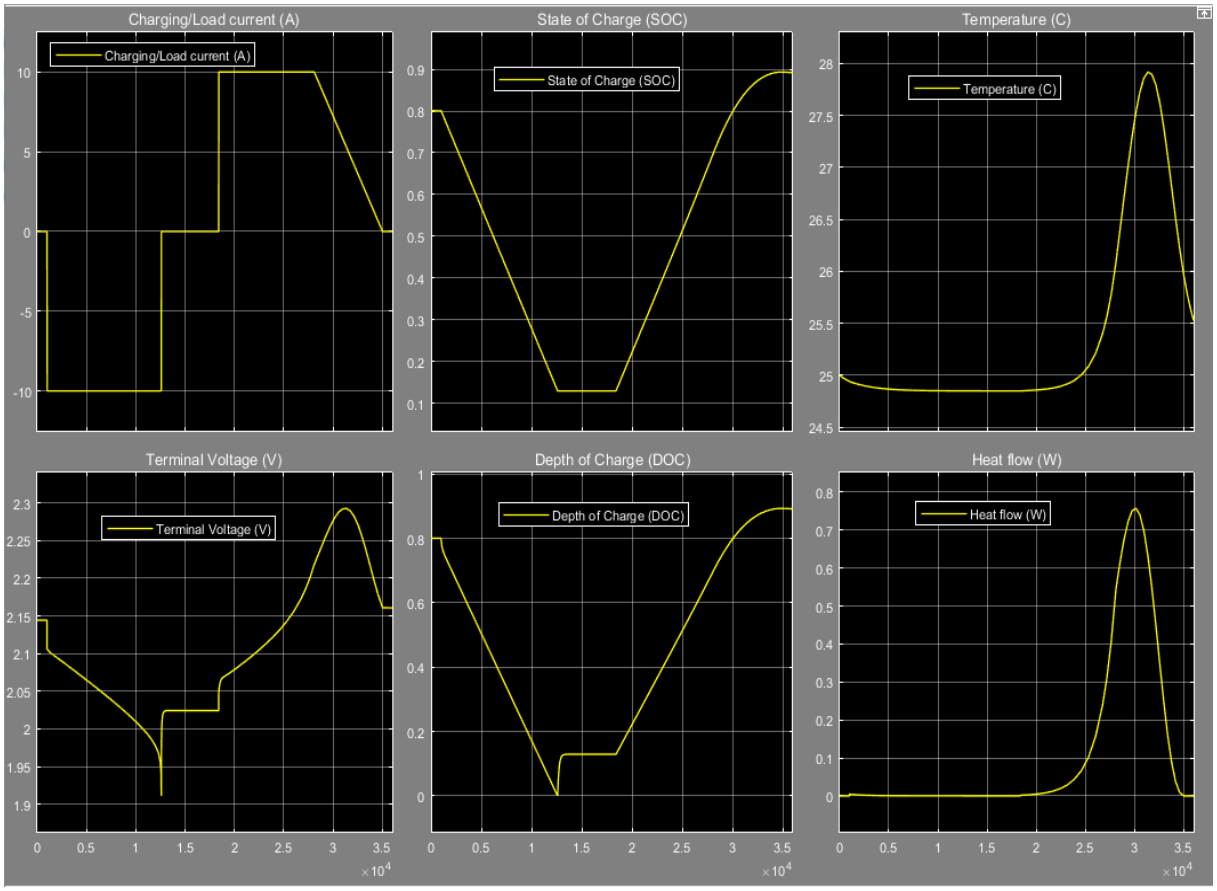

Figure 12: Simulation results at 25C (a) load current (b) SOC (c) temperature (d) terminal voltage (e) DOC and (f) heat flow (Jackey R. A.).

CHAPTER 3

METHODOLOGY

Battery storage is the costliest part of a PV-storage system. So, it is essential to predict the behavior of a battery to get the most out of it without compromising its lifetime. Battery modeling is a very complex procedure due to various electrical, chemical and thermal phenomena. For better understanding, we first studied some models like Li-ion and Lead-acid battery model. Then we developed our model using ANN (Artificial Neural Network) at different temperature level.

3.1 ANN-Predictive Thermal Batteries Models

This study describes Artificial Neural Network (ANN) application as one of the powerful artificial intelligence nonlinear regression techniques for batteries parameters estimation (El Shahat, Neural Network Storage Unit Parameters Modeling, 2014). ANN is a computational structure inspired by a biological nervous system.

3.1.1 Artificial Neural Networks (ANNs) Technique

An artificial neural network can be divided into three types of neuron layers (et, 2017).

(a) Input layer: This layer is responsible for receiving information (data), signals, or measurements from the outside condition. These inputs (samples or patterns) are standardized within the limit values produced by activation functions. This standardization brings about better numerical precision for the mathematical operations completed by the network.

(b) Hidden layers: These layers are made out of neurons which are responsible for extracting patterns associated with the process. These layers perform a large portion of the internal processing from a network.

(c) Output layer: This layer is also made of neurons and thus is liable for creating and presenting the final network outputs, which result from the processing performed by the neurons in the previous layers.

An ANN consists of elementary and closely interrelated processors called neurons or nodes. The neurons are associated with each other by weighted links over which signals can pass. Every neuron accepts more than one inputs signals from other neurons according to their construction weights and creates a single output which may transmit to several other neurons. Back-propagation learning algorithm has become the most popularly used technique in engineering application (El-Shahat, 2014). The main working procedure of a neuron is shown in figure 13.

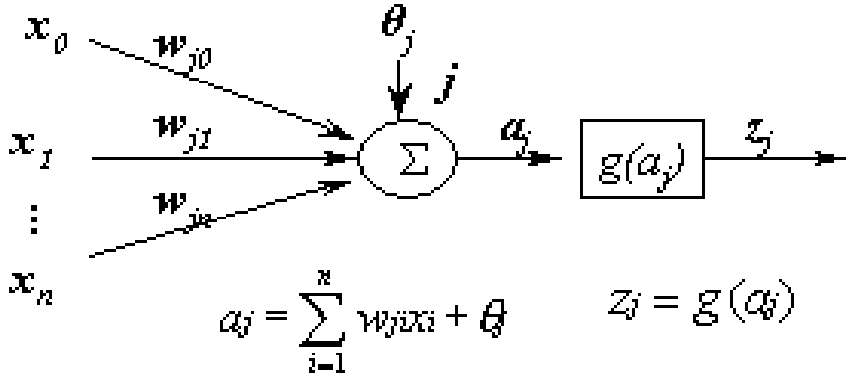

Figure 13: Neuron function (El-Shahat, 2014)

Figure 14 describes a feedforward network with multiple layers composed of one input layer with n sample signals, two hidden neural layers consisting of n1 and n2 neurons respectively, and, finally, one output neural layer composed of m neurons representing the respective output values.

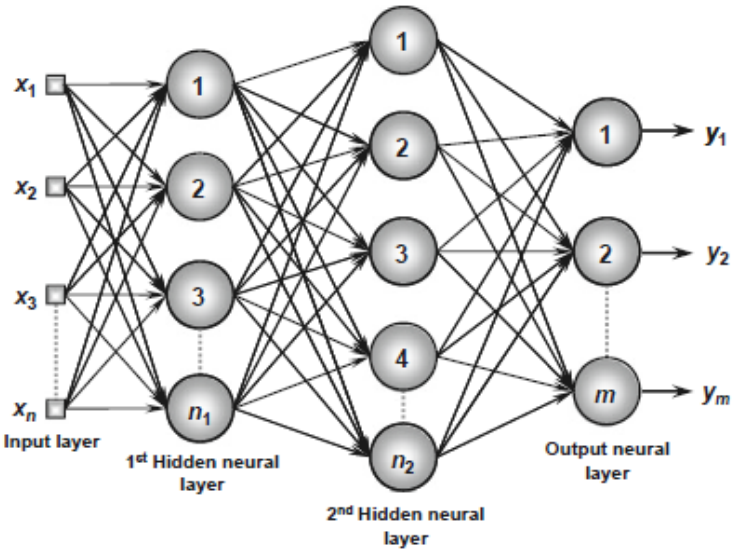

Figure 14: Example of a multiple layers feed-forward neural-network (Silva, Spatti, Flauzino, & Liboni, 2016)

The ANN modeling can be divided into two steps: (a) train the network and (b) test the network with data. A training set is a group of matched input and output patterns. It is necessary that all the information the network needs to learn to be supplied to the network as a data set. When each pattern is read, the network uses the input data to produce an output, which is then compared to the training pattern. If there is a difference, the connection weights are altered in such a way that the error is decreased. After the network has run through all the input patterns, if the error is still greater than the maximum desired tolerance, the ANN runs through all the input patterns repeatedly until all the errors are within the required tolerance. When the training reaches a satisfactory level, the network holds the weights constant, and the trained network can be used to make decisions or identify patterns in new data sets not used to train it.

An important issue in designing a network to decide the units in each layer. Using too few units can fail to detect the signals entirely in a complex data set, leading to under fitting. On the other hand, using too many units will increase the training time, perhaps so much that it becomes

impossible to train it completely in a reasonable period. The best number of hidden units depends on several factors such as the numbers of input and output units, the number of training cases, the amount of noise in the targets, the complexity of the error function, the network architecture, and the training algorithm. The best approach to find the optimal number of hidden units is trial and error.

3.2 Designing ANN Models

3.2.1 Design with ANN

Designing ANN models require some basic steps which are shown in figure 15.

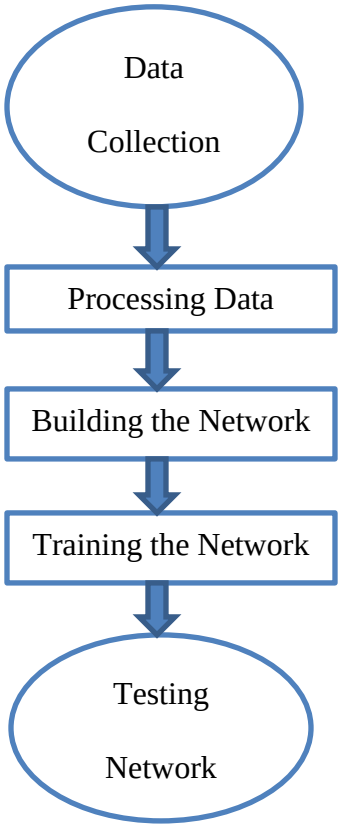

Figure 15: Flow diagram of ANN model

3.2.2 Data Collection

The first step of designing ANN model is to collect and preparing the data. Here we have collected data at different temperature level for both lithium-ion and a lead-acid battery.

3.2.3 Data Processing

To train the ANNS models more effectively there are three data processing ways. They are: (1) solve missing data problem, (2) to normalize the data and (3) to randomize the data. The average of neighboring values can replace the missing data. (Tymvios, Michaelides, & Skouteli, 2008).

3.2.4 Building the Network

In this step, a designer can define the number of hidden layers, neurons in each layer, transfer function in each layer, training function, weight/bias learning function, and performance function. In this work, multilayer perceptron (MLP) and linear networks are used (El-Shahat, 2014).

3.2.5 Training the Network

At the final step, the weights are accustomed to make the actual outputs close to the target outputs of the network. In this work, data at different temperature level are simulated to develop the MLP (multilayer perceptron) network.

3.2.6 Testing the Network

The final step is to test the performance of the developed model. At this stage, unseen data can be exposed to the model. For this study, values of temperature at different level have been used to test the ANN models.

3.3 Lithium-Ion Battery ANN Model

3.3.1 Li-Ion Battery Aging Model

Temperature always has a significant effect on battery performance, life cycle, safety and other parameters. Although, the extensive effects of temperature on the behavior of cycle aging rate of lithium-ion battery have yet to be determined. Based on the aging behavior of lithium-ion battery

we have developed an ANN model. Figure 16 represents the battery aging model using ANN. It has two inputs: temperature and cycle with eight outputs and hidden layers.

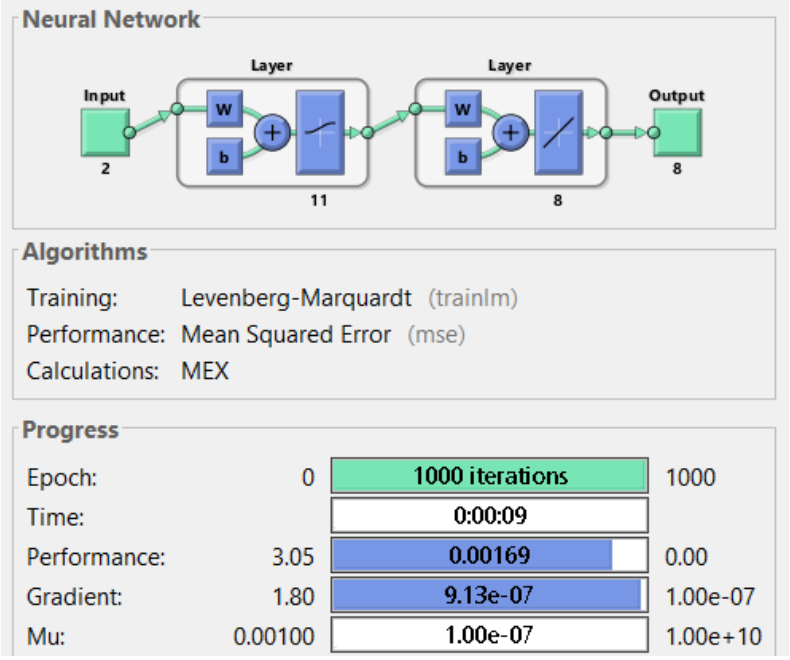

Figure 16: ANN aging model & design

In this work, network structure is designed with a log-sigmoid function in the hidden layer and a purely linear function in the output layer as shown in figure 16. The number of neurons in the hidden layer was selected to minimize the error to a desired performance level with the lowest possible number of neurons. For lithium-ion aging model, we have used eleven neurons for hidden layer one and eight neurons for hidden layer two. The number of neurons in hidden layer two must be equal to the number of outputs.

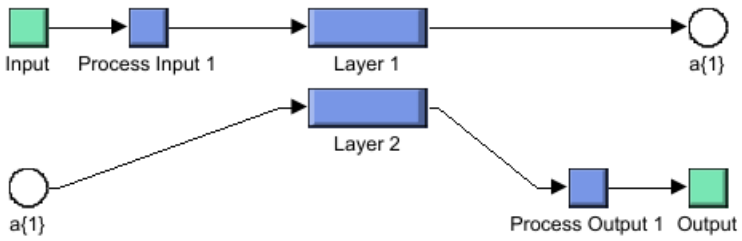

Figure 17: Network construction for aging model

Figure 17 describes the full network construction with input, output and two hidden layers.

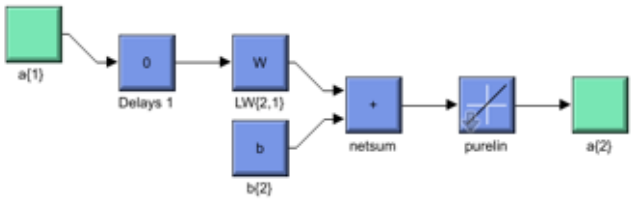

Figure 18: Hidden layer of aging model

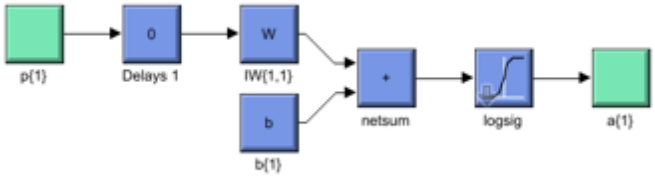

Figure 19: Output layer of aging model

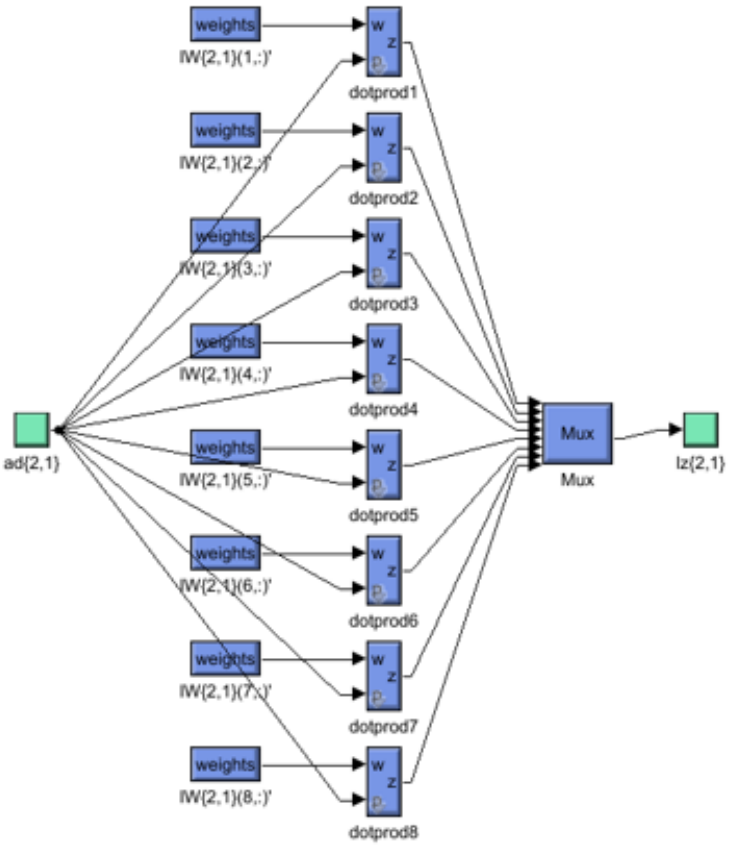

Figure 20: Output layer weights of aging model

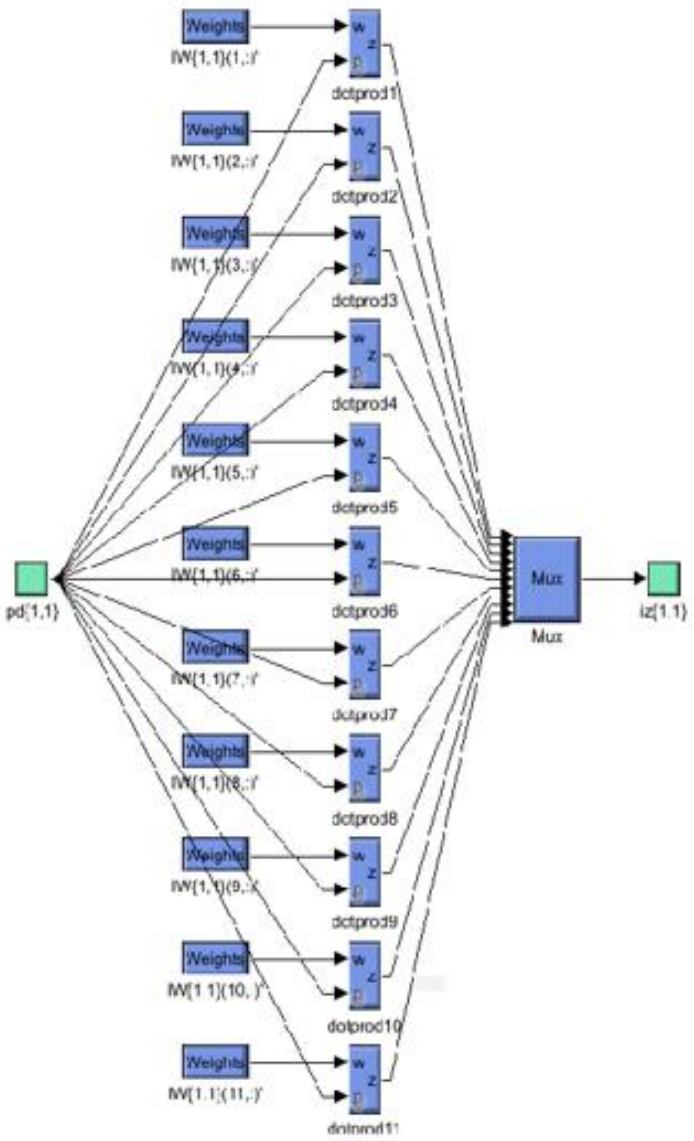

Figure 21: Hidden layer weights of aging model

Figure 18-21 shows the inside architecture of hidden layer one and two with the weighted links of eight and eleven neurons of corresponding hidden layer.

To train the ANN model 70% and 30% data used for training and testing set. Figure 22 represents the training state of lithium-ion battery aging model.

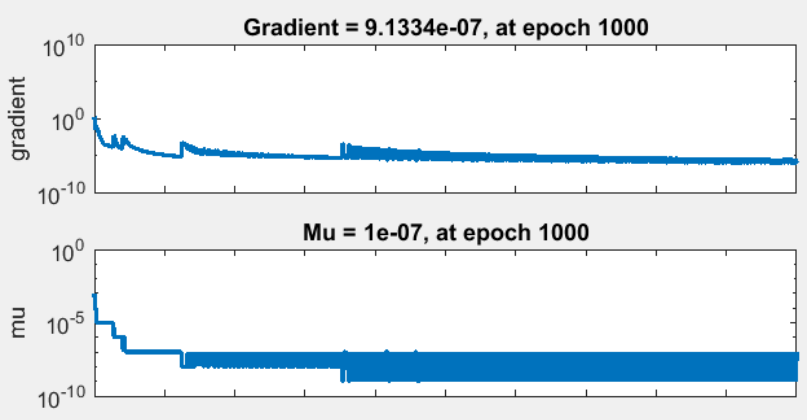

Figure 22: Training state of aging model

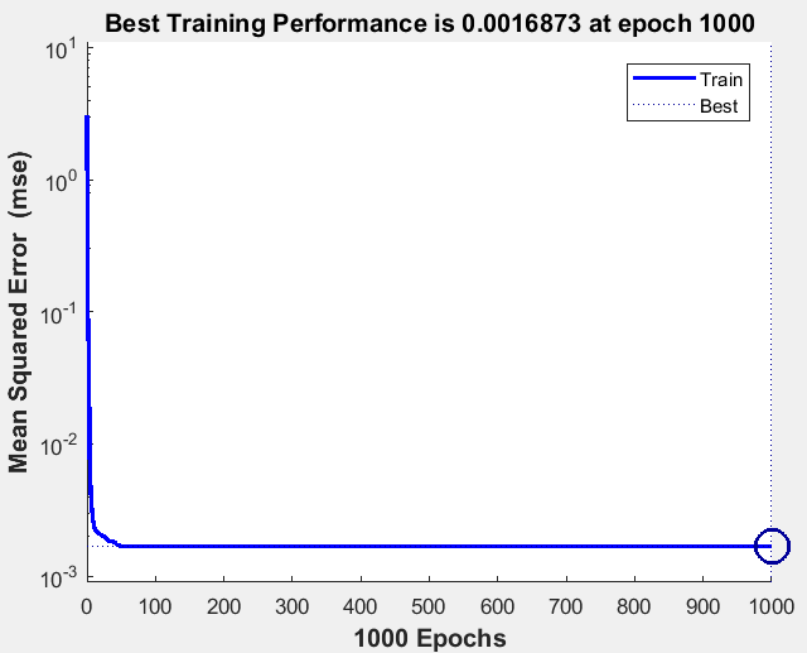

Figure 23: Mean square error of aging model

Figure 23 shows the mean square error which is used to optimize performance, and logistic sigmoid, linear network function was used to train the ANN. The mean square error (MSE) for this model was found to be less than 10^{-3} as shown in figure 23.

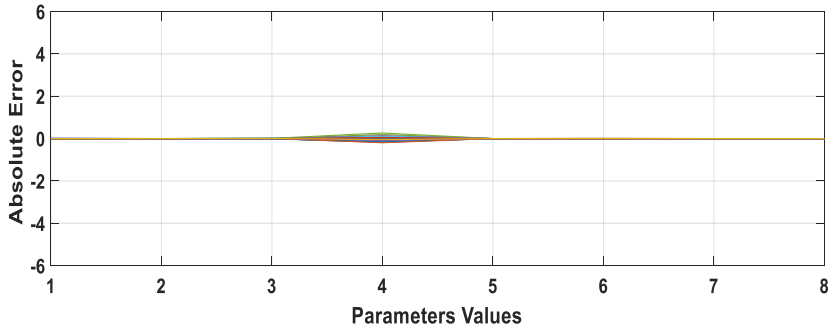

Figure 24: Absolute error for aging model

Figure 24 shows the absolute error for lithium-ion battery aging model.

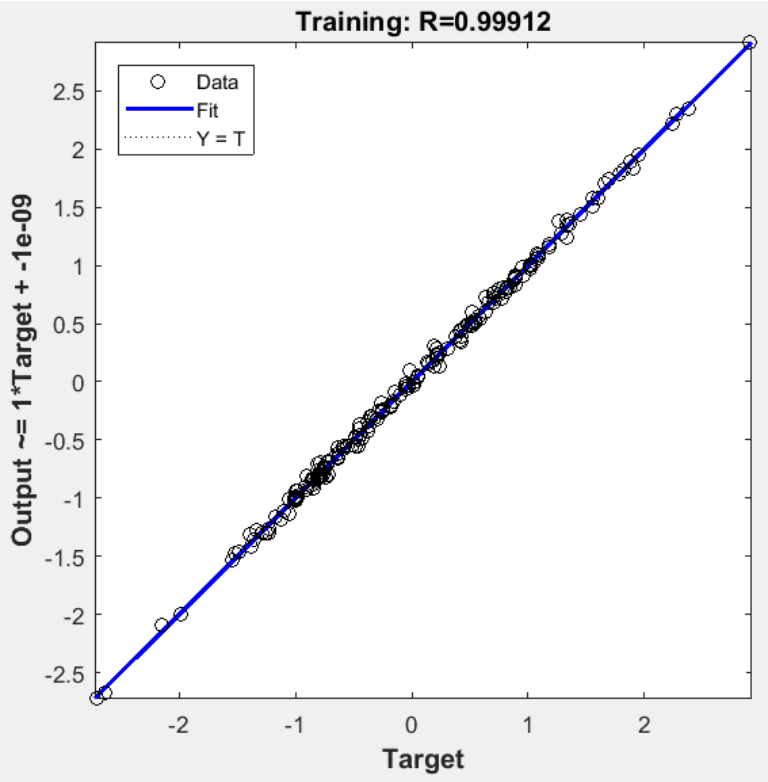

Figure 25: Regression factor for training data of aging model

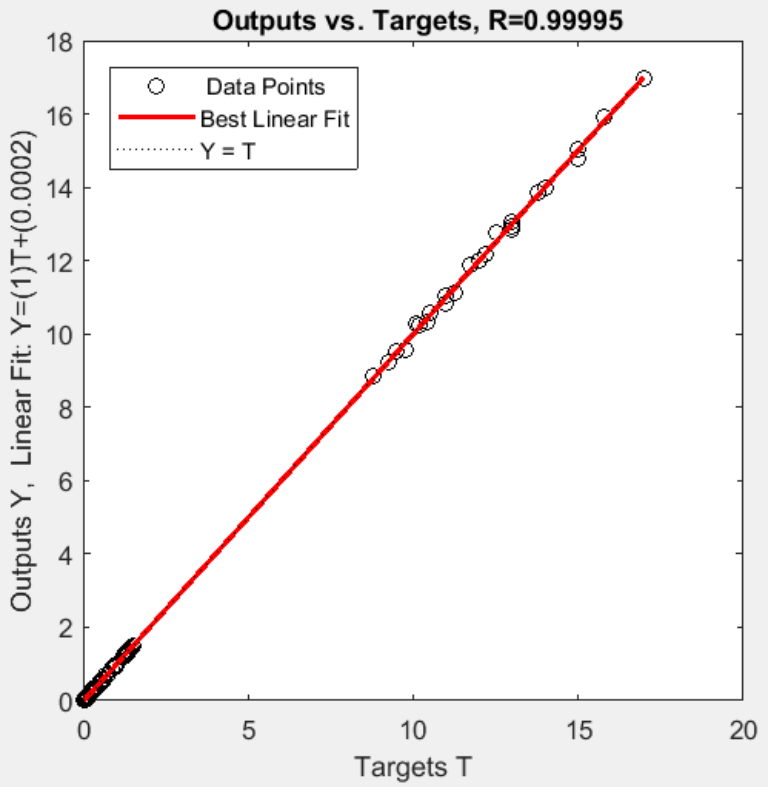

Figure 26: Comparison for the testing data of aging model

Figures 25 and 26 describe the comparisons between the training/testing data outputs and targets validating the model with a regression accuracy of 99.912%. Here the training and testing performance of the ANN model was 98.912% and 99.995% respectively using a feed-forward back-propagation technique (El-Shahat, 2014).

3.3.2 Li-Ion Battery Thermal Model

Figure 27 describes the model design using ANN. It has three inputs, two outputs with two hidden layers. For Li-ion battery temperature level was 5 to 35 degrees Celsius.

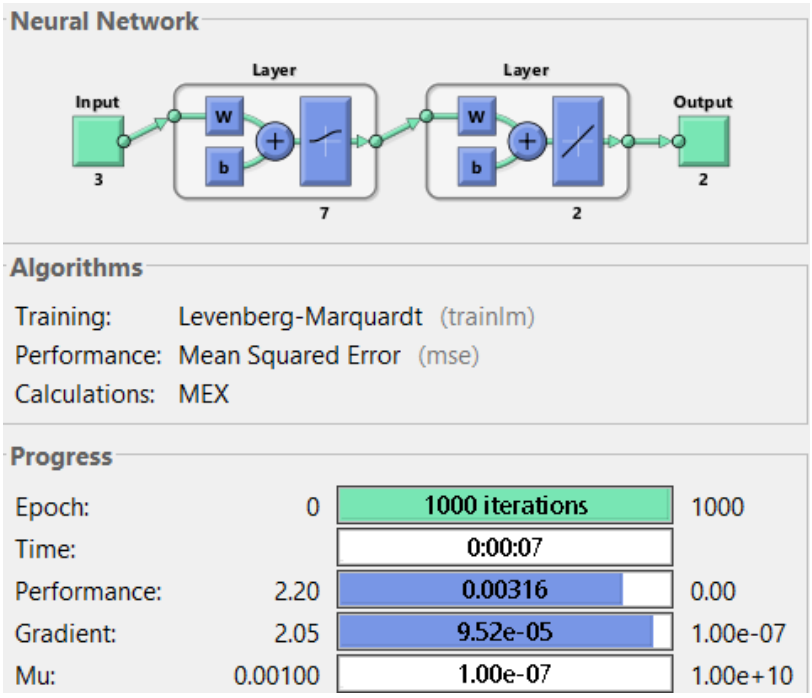

Figure 27: ANN model & design.

Here the network structure is a general approximator with a log-sigmoid function in the hidden layer and a purely linear function in the output layer as shown in figure 27. The number of neurons in the hidden layer was elected to minimize the error to a desired performance level with the lowest possible number of neurons. It is also increases the prediction accuracy of the model (El Shahat, Haddad, & Kalaani, An Artificial Neural Network Model for Wind Energy Estimation, 2015). For li-ion model, we have used seven neurons for hidden layer one and two neurons for hidden layer two. The number of neurons in hidden layer two must be equal to the number of outputs.

Figure 28 shows the full network construction with input, output, and two hidden layers.

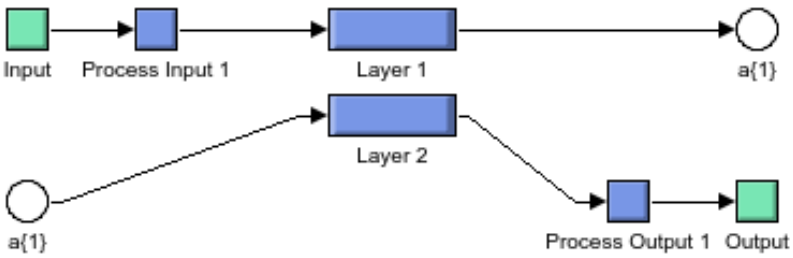

Figure 28: Network construction

Figure 29-32 shows the inside architecture of hidden layer one and two with the weighted links of seven and two neurons of the corresponding hidden layer.

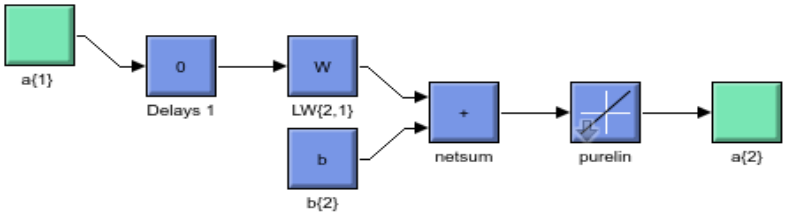

Figure 29: Hidden layer

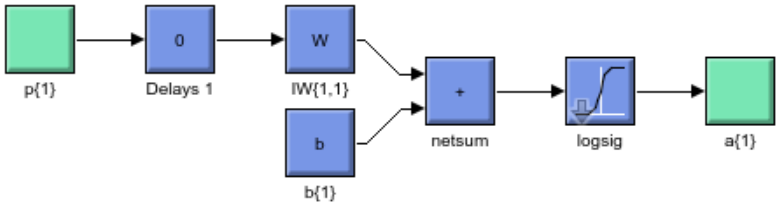

Figure 30: Output layer

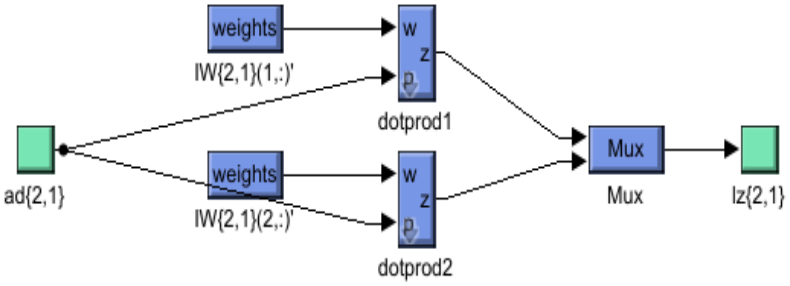

Figure 31: Output layer weights

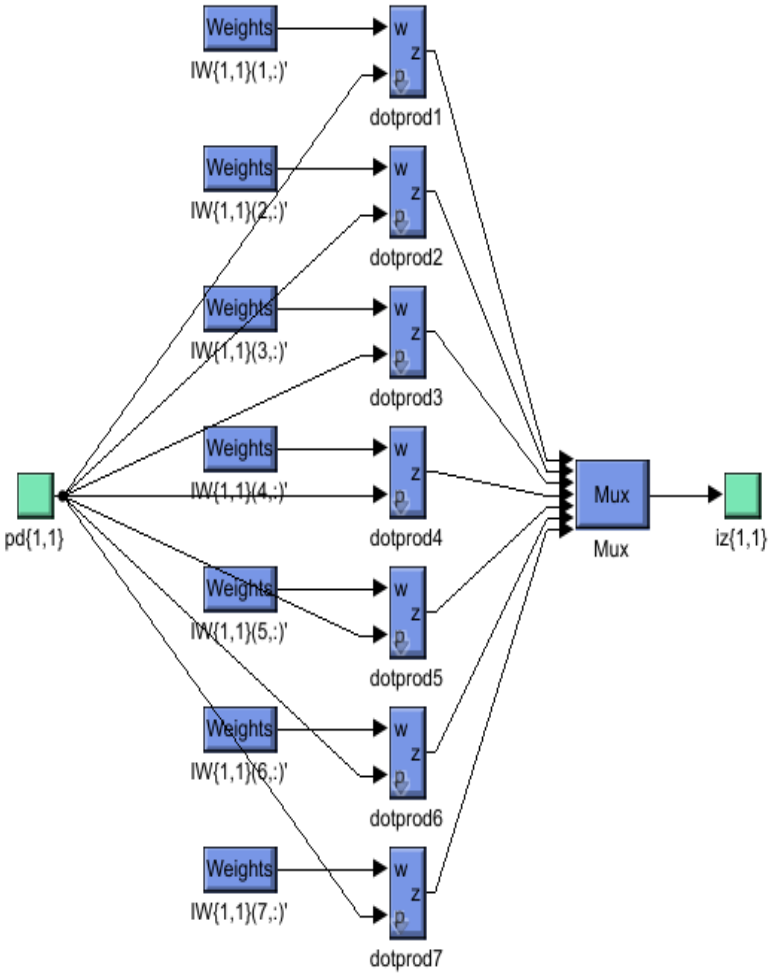

Figure 32: Hidden layer weights

Figure 31 & 32 represents the Simulink model used in the sizing process. A set of algebraic equations used to generate the sizing parameters without the need for retraining the network every time. To train the ANN model 70% and 30% data used for training and testing set.

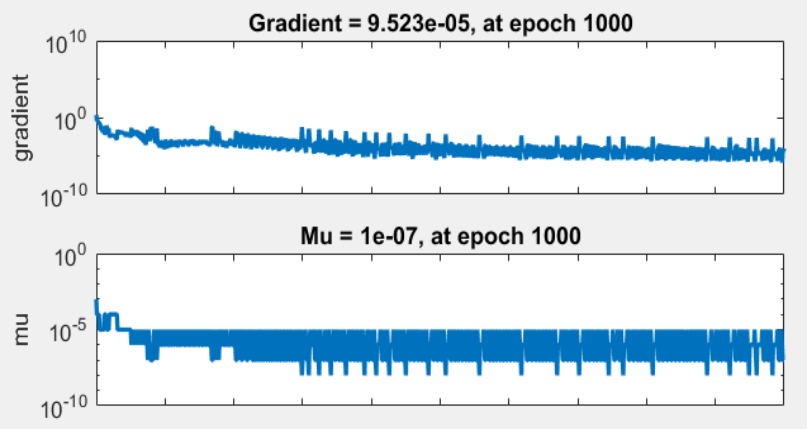

Figure 33: Training state

Figure 34 shows the mean square error which is used to optimize performance, and logistic sigmoid, linear network function was used to train the ANN. The mean square error (MSE) for this model was found to be less than 10^{-3} as shown in figure 34.

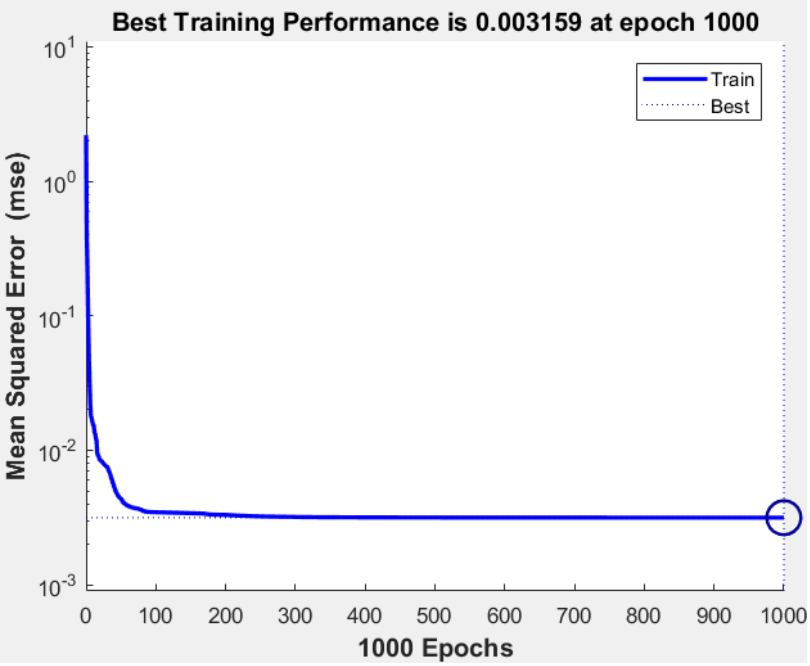

Figure 34: Mean square error

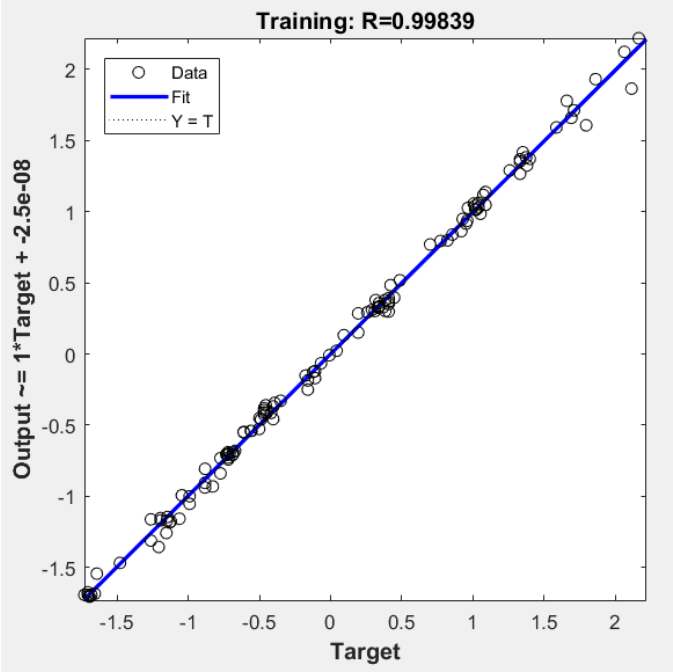

Figure 35: Regression factor for the training data

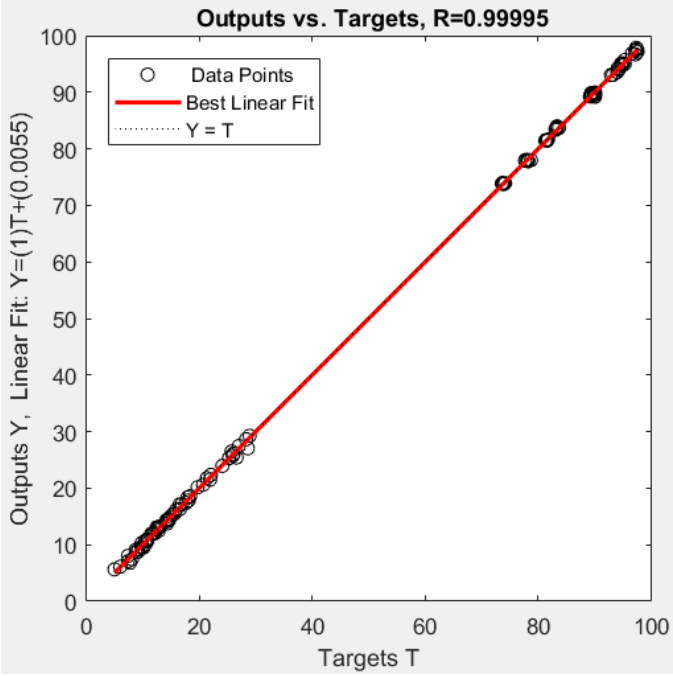

Figure 36: Comparison for the testing data

Figures 35 and 36 illustrate the comparisons between the training/testing data outputs and targets validating the model with a regression accuracy of 99.839%. Here the training and testing

performance of the ANN model was 98.839% and 99.995% respectively using the feed-forward back-propagation technique (El-Shahat, 2014).

3.3.3 Lead-Acid Battery ANN Model

Figure 37 describes the model design using ANN. It has three inputs, five outputs with two hidden layers. For lead-acid battery temperature level was -5 to 75 degrees Celsius.

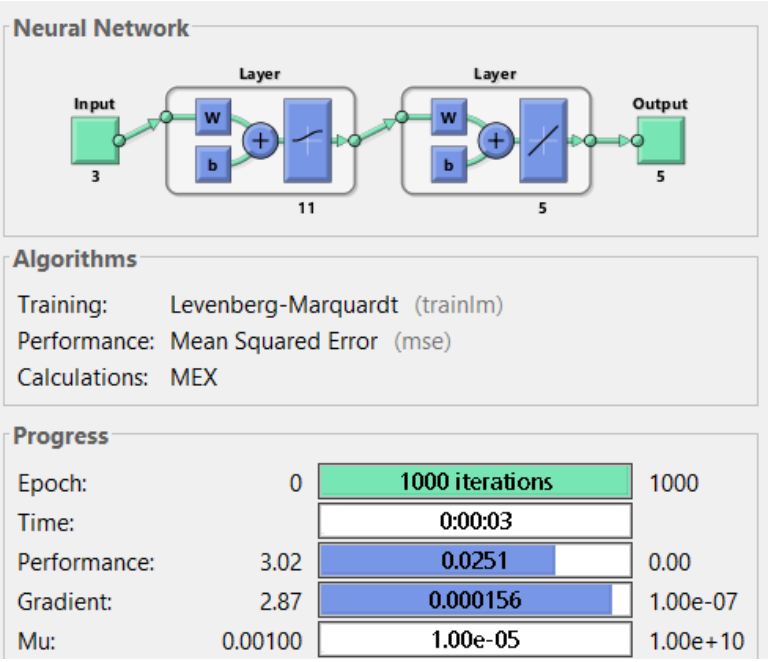

Figure 37: ANN model & design

Here the model configuration is a multilayer network with a log-sigmoid function in the hidden layer and a purely linear function in the output layer as shown in figure 37. The number of neurons in the hidden layer was selected to minimize the error to a desired performance level with the lowest possible number of neurons. It is also increases the prediction accuracy of the model (El Shahat, Haddad, & Kalaani, An Artificial Neural Network Model for Wind Energy Estimation, 2015). For lead-acid model, we have used eleven neurons for hidden layer one and five neurons for hidden layer two. The number of neurons in hidden layer two must be equal to the number of outputs.

Figure 38 shows the full network construction with input, output, and two hidden layers.

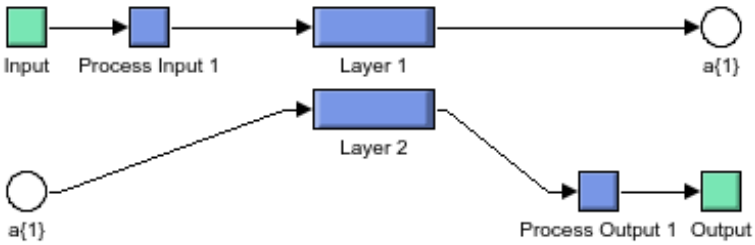

Figure 38: Network construction

Figure 39-42 shows the inside architecture of hidden layer one and two with the weighted links of eleven and five neurons of the corresponding hidden layer.

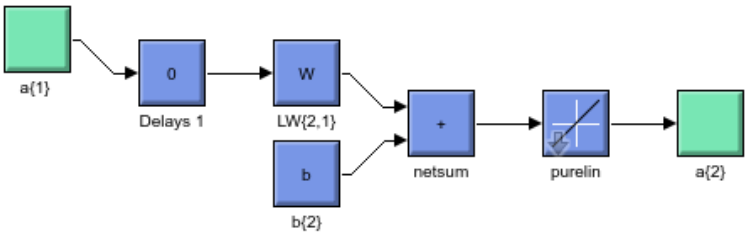

Figure 39: Hidden layer

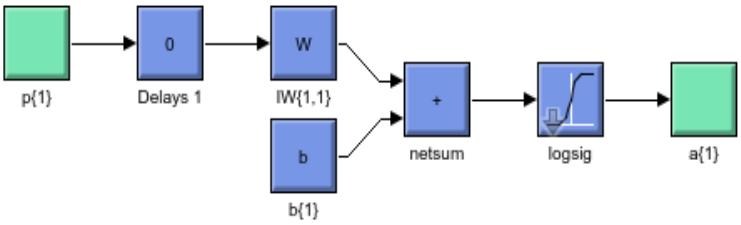

Figure 40: Output Layer

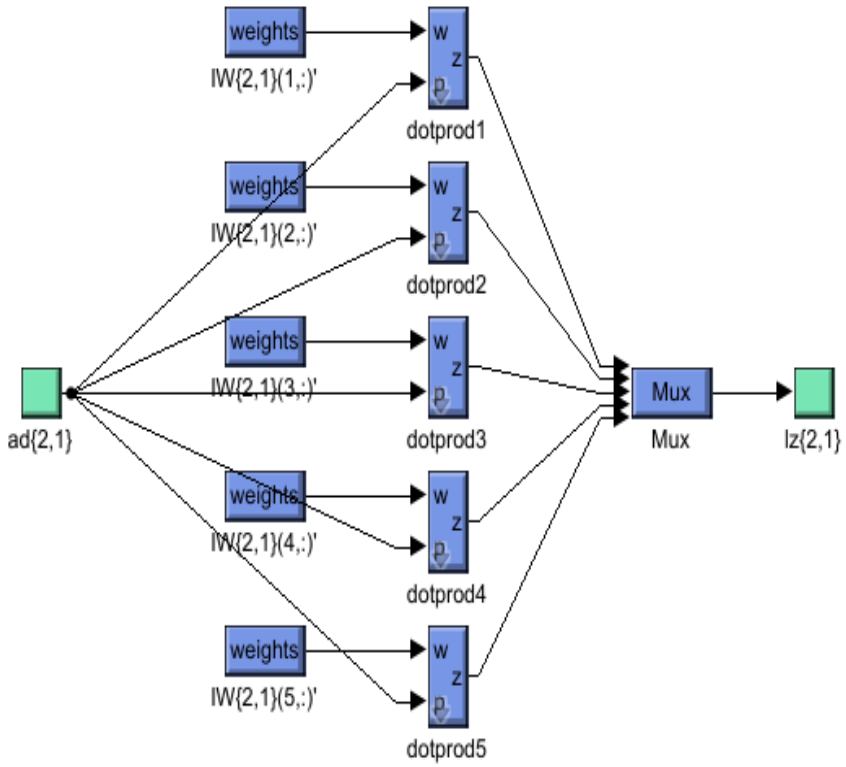

Figure 41: Output layer weights

Figure 41 & 42 depicts the Simulink model used in the sizing process. A set of algebraic equations used to generate the sizing parameters without the need for retraining the network every time.

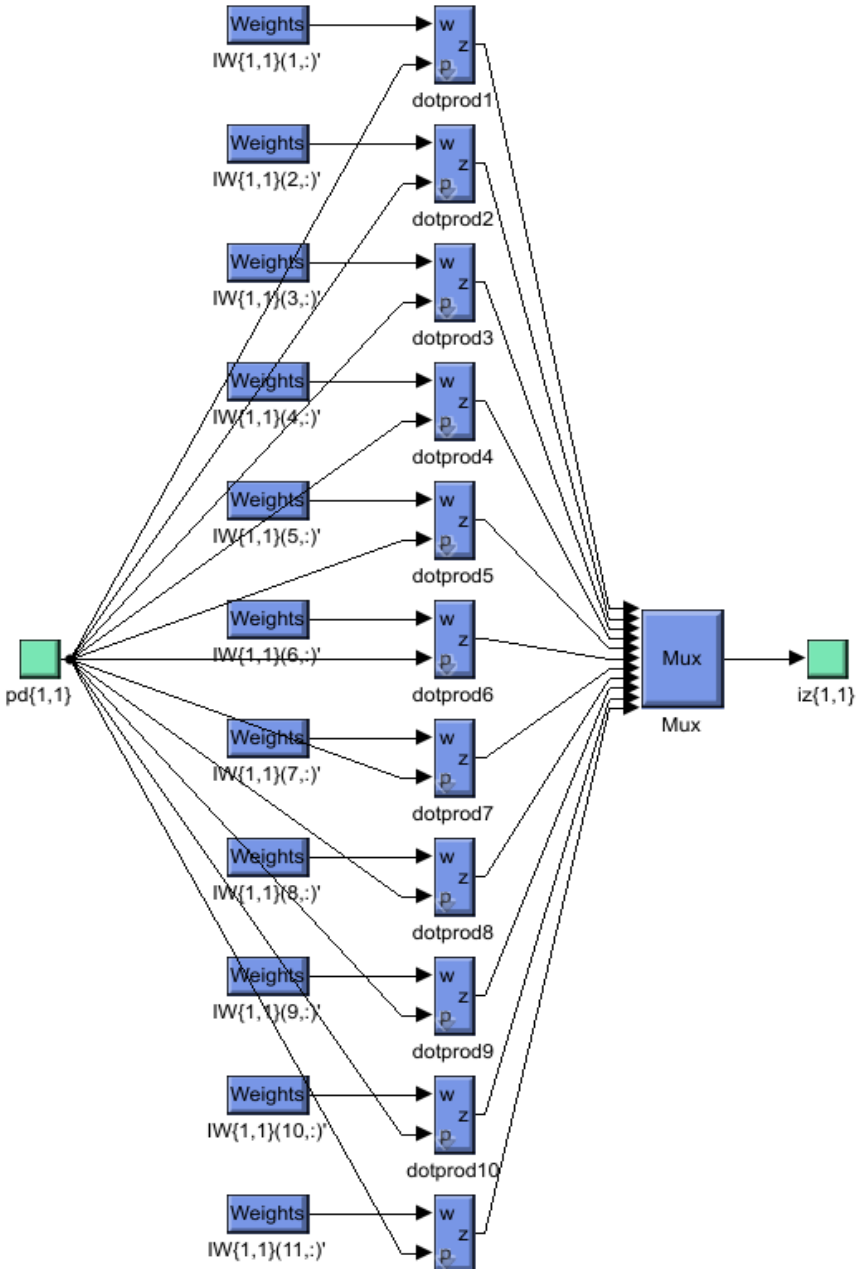

Figure 42: Hidden layer weights

To train the ANN model 70% and 30% data used for training and testing set.

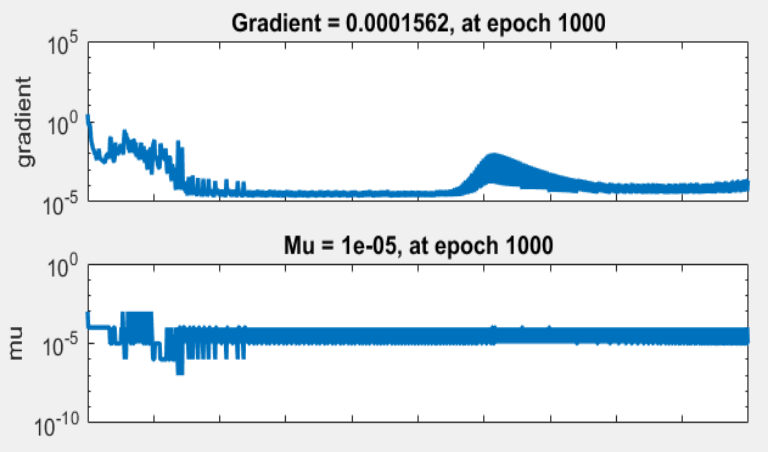

Figure 43: Training state

Figure 44 shows the mean square error which is used to optimize performance, and logistic sigmoid, linear network function was used to train the ANN. The mean square error (MSE) for this model was found to be less than 10^{-2} as shown in figure 44.

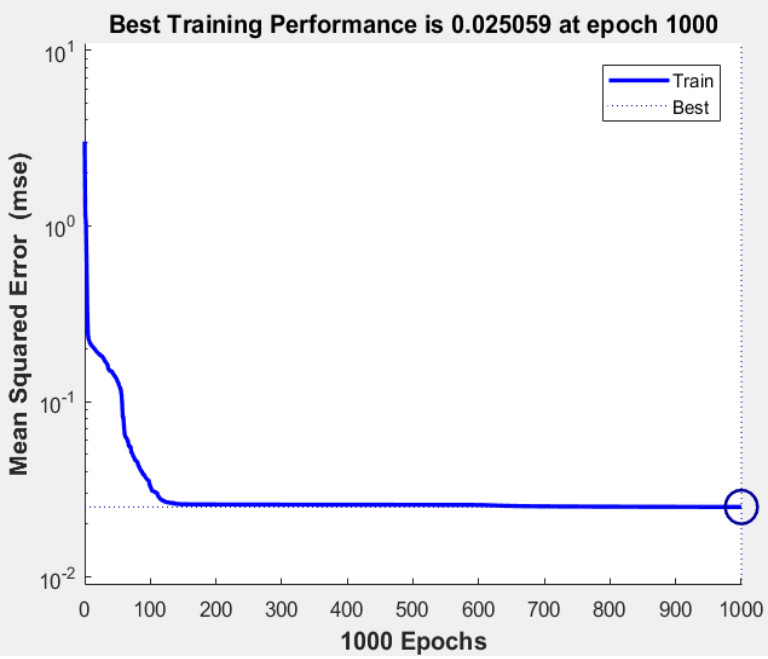

Figure 44: Mean square error

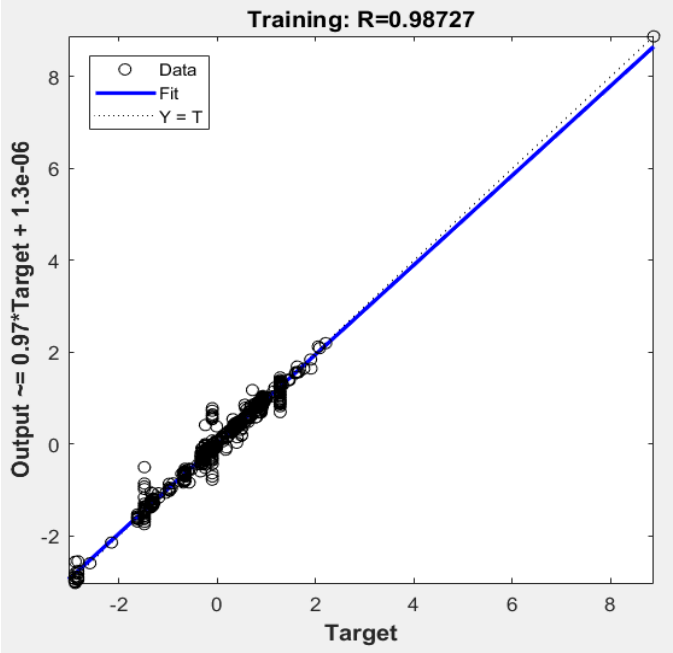

Figure 45: Regression factor for the training data

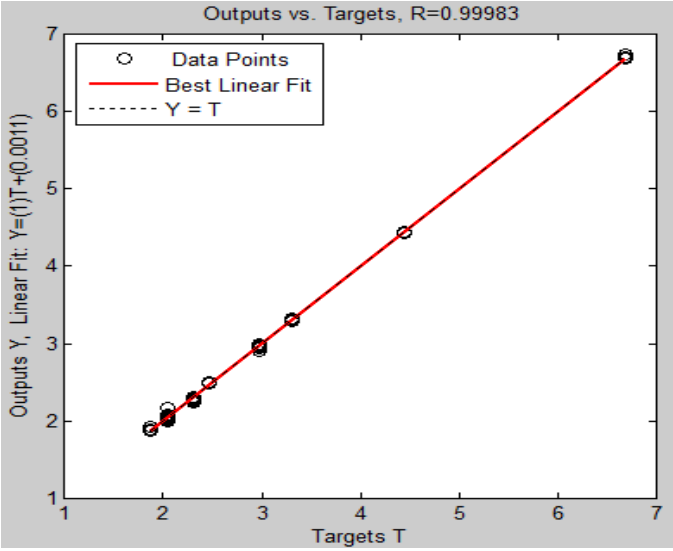

Figure 46: Comparison for the ANN model testing data

Figures 45 and 46 illustrate the comparisons between the training/testing data outputs and targets validating the model with a regression accuracy of 98.727%. Here the training and testing

performance of the ANN model was 98.727% and 99.983% respectively using the feed-forward back-propagation technique (El-Shahat, 2014).

3.4 HOMER Simulation

In this study, we created a HOMER (Hybrid Optimization of Multiple Energy Resources) simulation model using lithium-ion and lead-acid battery to measure cost-effectiveness and comparison with other energy storage devices.

3.4.1 Solar and Wind Availability

The radiation which is available on earth's surface can be calculated in many ways. The radiation is calculated based on immediate normal irradiance (DNI) and Global Horizontal Irradiance (GHI). GHI is typically measured with a pyranometer and DNI with a pyrheliometer (Reno, Hansen, & Stein, 2012) . The wind asset shifts with each day and the period of the year as well as some degree from year to year. Wind turbine takes an average power output characteristic which depends on the producer's determinations. Wind turbine begins creating power at the cut-in speed and power yield increments straightly with the variety of twist speed from cut-in to evaluate speed. The power acquired from the wind turbine can be written as

$$P_w = \frac{1}{2}\,\rho\pi R^2 C_p V^3 \tag{3.1}$$

Where, ρ is the air density (ρ=1.225 kg/m^3), R is the blade length, and V is the wind speed (Sarkar & Khule, 2016). Here, we used one wind turbine generator. The power curve is the most vital property of the wind turbine, which represents the measure of force the turbine produces versus wind speed.

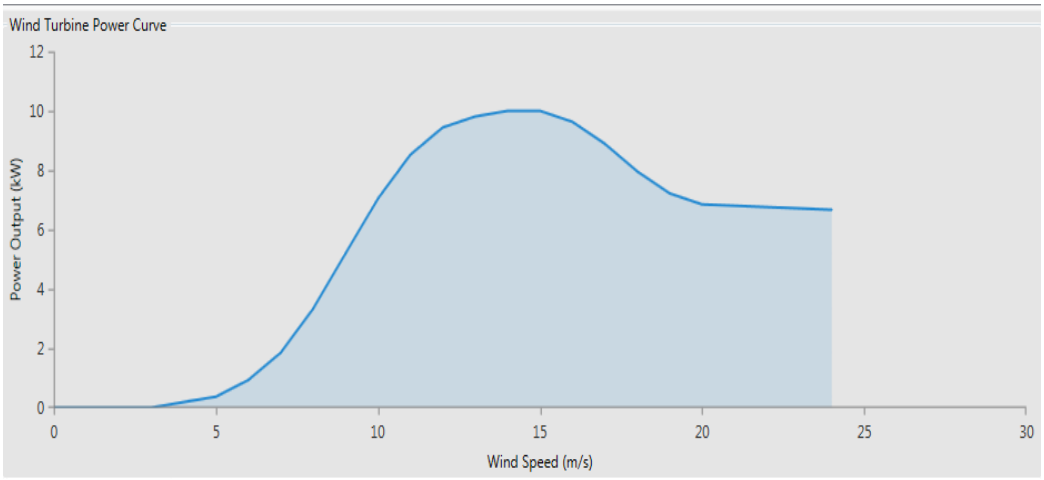

Figure 47: Power curve for 10 kW AC

3.4.2 Data Collection

Solar and wind speed data are acquired from NASA for Statesboro, Georgia. As displayed in HOMER, the latitude and longitude of this place are $32^{\circ}26.9'N, 81^{\circ}47.0'W$ respectively. Figure 48(a,b) presents the average-daily-irradiance per month for 6.4 to 7.8 (kW/m^2) range and the average daily wind speed per month.

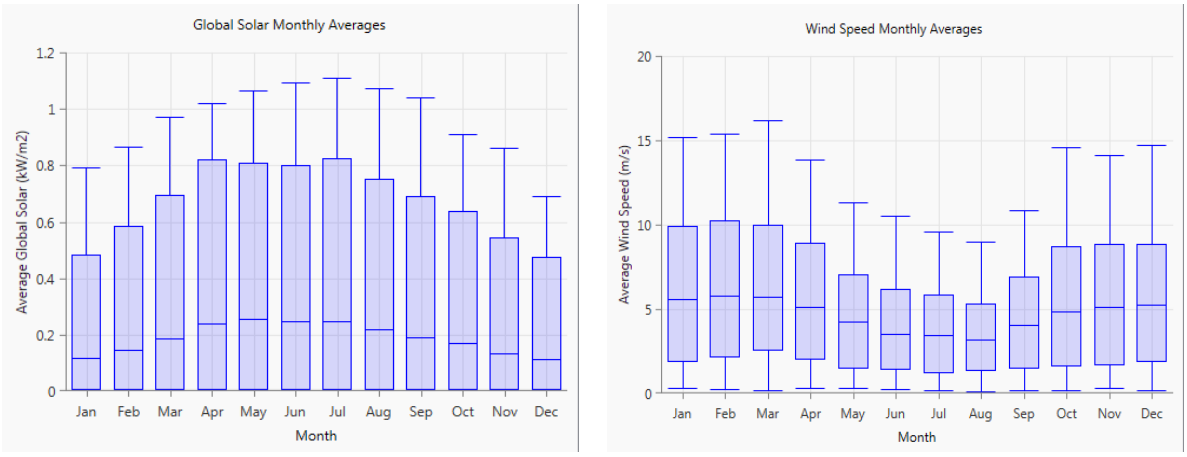

(a) (b)

Figure 48: (a) Average-daily-sun-irradiance per month, (b) Average-daily-wind-speed per month

3.5 HOMER Simulation Model

HOMER, software is used for evaluations in both stand-alone and grid-connected systems (Givler & Lilienthal, 2005) (lilienthal, Gilman, & Lambert, 2005).

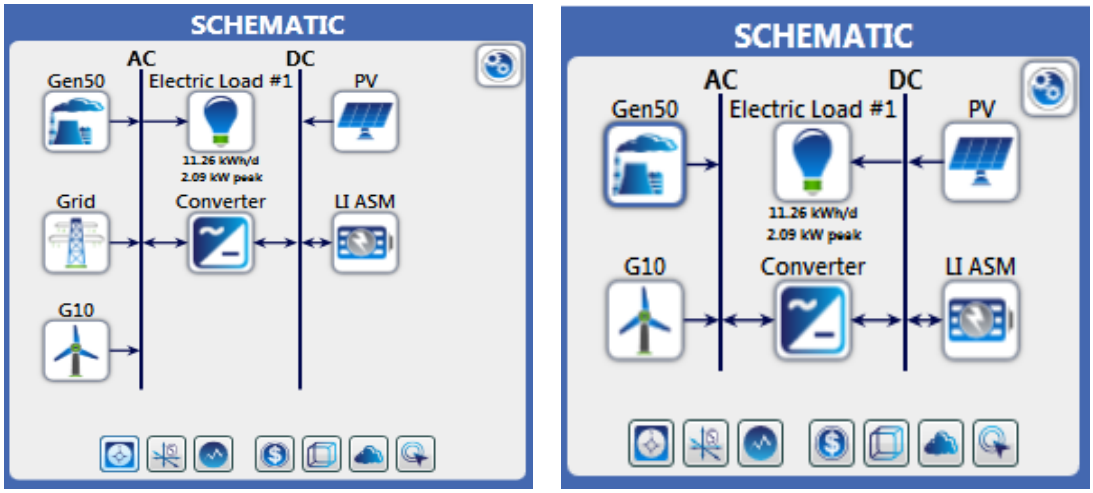

(a) (b)

Figure 49: (a) Framework arrangement in HOMER (grid connected), (b) Framework arrangement in HOMER (off-grid)

Figure 49 represents the Hybrid Power System Design using HOMER. This model consists of Generic flat plate PV, Generic 10 kW wind turbine, 50 kW generator, converter, residential load and Generic 1kWh Li-ion battery. In normal operation hour, PV and wind turbine feed the load demand while the extra energy from these components is stored in these batteries.

The simulation procedure fills two needs. Firstly, it checks all feasibility of the system. HOMER considers the model to be workable if it can sufficiently serve the electric load and fulfill some other requirements forced by the client. Secondly, the life-cycle cost of the system configuration is resolved, which is the total cost of installing and operating the system over its life span. To evaluate the system performance under various operating conditions, simulation processes have been carried out using HOMER built-in data (NASA Surface meteorology and Solar Energy)

which is calculated based on location. During optimization, HOMER simulates a various combination of the system and avoid the results which are not feasible. Then it shows the feasible results based on total net present cost (NPC). From these results, we can choose the feasible output with minimum net present cost. Optimization process decides the optimum value of every different result that interest the modeler (Giraud & Salameh, 2001).

For optimum cost calculation, HOMER simulates both off-grid and on-grid design under the same load. Here, we used the following input parameters.

3.5.1 Generic Flate Plate PV

This photovoltaic array is flat plate type and manufactured by Generic.

3.5.2 Wind Turbine

In this paper, Generic 10 kW wind turbine is used.

3.5.3 Storage Device

Here we used Generic 1kW Li-ion which is a modified kinetic model battery. It includes rate dependent losses, temperature dependence on capacity, cycle lifetime estimation using Rainflow counting and temperature effect on calendar life. Additionally, it can support the system in off-grid mode. From the following cost curve, we can see that, by adding different quantity we can vary the cost which will eventually make an effect on total net present cost (NPC).

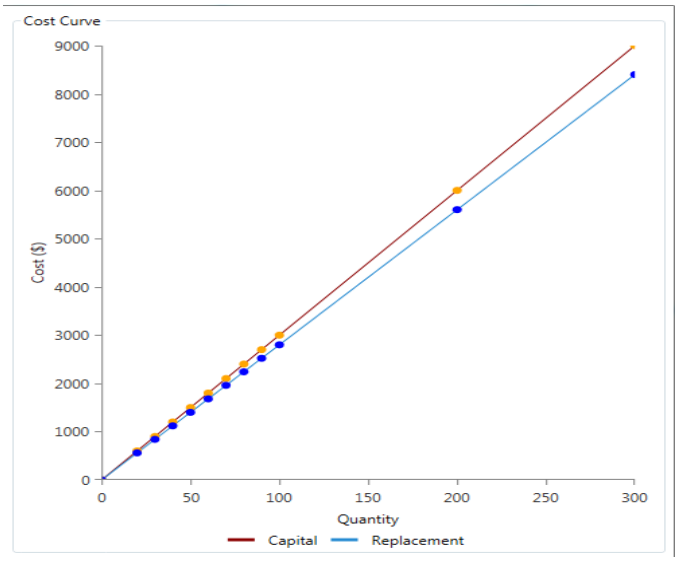

Figure 50: Cost curve of Li-ion battery

3.5.4 System Converter

It is a system converter manufactured by Generic.

3.5.5 Advanced Grid

When there is insufficient power, the grid supplies power to fulfill the load demand. On the other hand, it consumes power when excessive power is available.

TABLE 3.1 TECHNICAL DATA FOR HOMER MODEL

Input Parameters	Wind Turbine	PV Module	Converter	Li-ion Battery
Capital Cost ($)	2000	4615	420	30
Replacement Cost ($)	1540	3692	350	28
O & M ($)	8	8	1	1
Lifetime(year)	20	25	15	-
Efficiency (%)	-	13	90	-
Hub Height (meter)	24	-	-	-
Operating temperature (°C)	-	47	-	-
Derating Factor (%)	-	80	-	-

Input Parameters	Wind Turbine	PV Module	Converter	Li-ion Battery
Initial SOC (%)	-	-	-	100
Minimum SOC (%)	-	-	-	20
Capacity Degradation Limit (%)	-	-	-	30
Nominal Voltage	-	-	-	3.7
Nominal Capacity(kwh)	-	-	-	1
Maximum Capacity(Ah)	-	-	-	276

3.5.6 Optimization Outputs

In this study, we have considered residential load. Assuming that, the lifetime of the whole project is 25 years. Figure 51 and 52 show the optimization results for our proposed model with and without grid connection respectively. The optimization process is carried out through every possible selection of variables in this hybrid power system without considering the sensitivity variables (U., P. S., & A. P. S., 2012).

From figure 51 there are two optimized results, the second one has no contribution from wind resource which results in more dependency on solar energy. So, we can ignore this combination. The first result has contributions from all the energy sources. Additionally, it costs least for per kWh energy. On the other hand, from figure 52, we can see that, for off-grid connection, we have selected the second result as it has contributions from all the energy sources.

The minimum COE obtained from the result is $0.0618. In this scenario, the percentage of renewable energy contribution is 98%. In the proposed grid connected model, an optimum number of renewable energy sources is activated and supplies electricity to the load. From figure 51 & 52, it can be clearly seen that off-grid power system for the same load is more expensive

($1.11) than grid-connected system ($0.0618). The NPC (net present cost) for on-grid and off-grid design is $34,660 and $58,714 respectively.

Architecture												Cost				System
						PV (kW)	PV-MPPT (kW)	G10	Gen50 (kW)	LI ASM	Grid (kW)	Converter (kW)	Dispatch	COE ($)	NPC ($)	Operating cost ($)	Initial capital ($)	Ren Frac (%)
						25.0	25.0	1	100	20	999,999	28.0	CC	$0.0618	$34,660	-$1,246	$50,770	98
						25.0	25.0		100	20	999,999	28.0	CC	$0.0770	$37,235	-$892.30	$48,770	95

Figure 51: Screenshot of optimized results (grid connected)

Architecture											Cost				System
					PV (kW)	PV-MPPT (kW)	G10	Gen50 (kW)	LI ASM	Converter (kW)	Dispatch	COE ($)	NPC ($)	Operating cost ($)	Initial capital ($)	Ren Frac (%)
					25.0	25.0		100	20	28.0	CC	$1.06	$56,397	$589.96	$48,770	100
					25.0	25.0	1	100	20	28.0	CC	$1.11	$58,714	$614.54	$50,770	100

Figure 52: Screenshot of simulation for finding optimal design (without grid)

Production	kWh/yr	%
Generic flat plate PV	39,523	83.51
50kW Genset	0	0.00
Generic 10 kW	6,774	14.31
Grid Purchases	1,033	2.18
Total	47,329	100.00

Consumption	kWh/yr	%
AC Primary Load	4,110	9.47
DC Primary Load	0	0.00
Grid Sales	39,281	90.53
Total	43,391	100.00

Figure 53: Snapshot of electricity production & consumption

According to figure 53 total yearly production of our proposed model is 47,329 kWh/yr and consumption for residential load 43,391 kWh/yr. Then we can sell the rest of the production to the grid. Monthly average electricity production from various parameters is shown in figure 54. It is clear that most of the contribution came from solar irradiance.

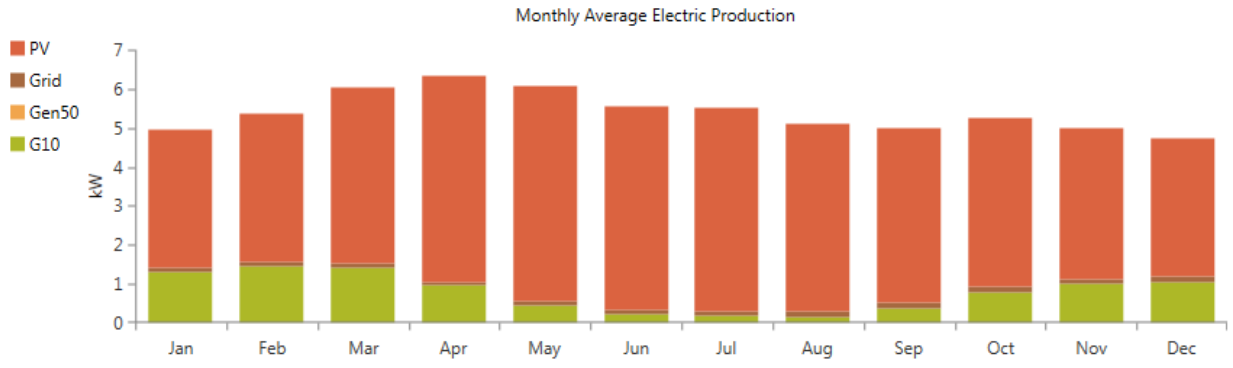

Figure 54: Snapshot of monthly average electricity production

Table 3.2 describes various cost parameters used for this simulation of lithium-ion battery.

Table 3.2 OPTIMIZED ANALYSIS FOR THE COST

Component	Capital ($)	Replacement ($)	O&M ($)	Fuel ($)	Total ($)
Generator	1600	0	0	0	1249.65
Wind Turbine	2000	490.96	103.43	0	2314.70
Battery	600	237.59	258.54	0	1051.41
PV	23,075	0	517.11	0	23,592.11
Converter	420	148.50	12.91	0	553.46
System	50,770	8,709.14	22,645.75	0	34,659.6

This study represents a comparison between a stand-alone and a grid-connected hybrid system for Statesboro without considering the effect of sensitivity variables (U., P. S., & A. P. S., 2012). The simulation results show that, grid-connected hybrid power system which includes solar and wind is more cost-effective than without grid-connected system for the same load. Our designed HOMER model is more cost-efficient as our energy-cost-effective (COE) is 0.0618$/kWh, and the average residential electricity rate in Statesboro is 0.116$/kWh (Electricity Local, n.d.).

3.6 Comparison of Distinct Types of Storage Devices using HOMER

To make power networks more intelligent and encouraging with incorporation of renewable energy sources, storage devices are acknowledged as the essential initiative to accomplish a safe power sector (Loh, Chai, & Blaabjerg, May 2013) (Boroyevich, Cvetkovic, Burgos, & Dong, Intergrid: A Future Electronic Energy Network, Sept 2013). As fossil powers, for example, coal, oil is exhausting day by day, renewable energy sources have been urged to guarantee energy security of the entire world. Within 2040, non-hydropower renewable energy sources will represent more than 66% of the total renewable era, while on the other hand, the total renewable share of all power era will increment from 13% in 2013 to 18% in 2040 (Annual Energy Outlook, April 2015). To store the energy, we need a backup system. For this reason, several types of batteries like Li-ion, Lead-acid and Vanadium continue being the favored choice.

A battery can convert stored chemical energy into electrical energy with some internal heat losses (Xing, Ma, Tsui, & Pecht, 2011). Maximum capacity of a battery can be determined by SOC (state of charge), SOH (state of health) and SOF (state of function). SOC of a cell is the percentage of its total energy capacity that is still available to discharge while on the other hand, SOH describes the present condition and ability to deliver the specified performance compared with a new battery (Zhang, Lee, & Huang, 2014). Li-ion batteries have greater power in a smaller package. It has fundamentally higher life cycle than a lead acid battery in the field of discharge. Lead acid batteries require ordinarily more crude material than lithium-particle to accomplish a similar energy storage, having a substantially bigger effect on the earth amid the mining procedure (Albright, edie, & Al-Hallaj, 2012). In case of vanadium redox flow battery, it has low power and energy densities which suggest more complex system compared to other storage batteries (Guarnieri, Mattavelli, Petrone, & Spagnuolo, Dec 2016).

Here, we have designed three diverse types of battery model using HOMER which are Li-ion, Lead-acid and Generic Vanadium. Solar & wind data is acquired from NASA Surface meteorology and Solar Energy for the location of Statesboro, Georgia. The previous figure 48 shows the monthly average daily solar radiation and wind speed.

3.7 Correlation of Technical Parameters

3.7.1 Storage Devices

Here we used Generic 1kW Li-ion, Lead-acid & Generic Vanadium which is modified kinetic model battery. From the following figure of the cost curve, it is observed that by adding different quantity total net present cost (NPC) can be varied.

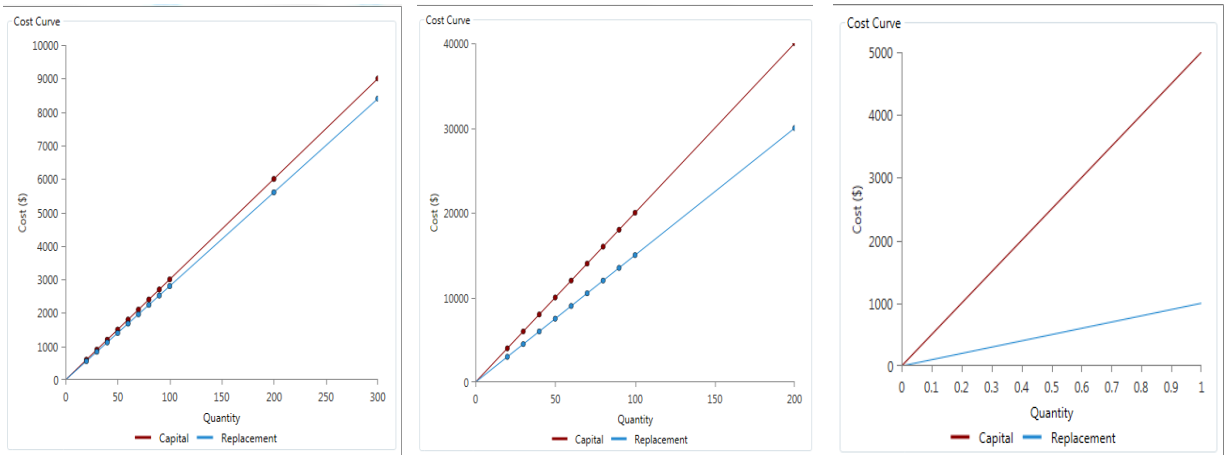

(a) (b) (c)

Figure 55: Cost curve for (a) 1 kW Li-ion (b) 1 kW Lead-acid (c) Generic Vanadium

3.7.2 Charging Time

There are three types of Li-ion battery: cobalt, manganese, and phosphate. The time required for a full charge is 2-4h, 1h or less, 1h or less respectively while for lead-acid time is varied from 8-16 hours (Diouf & Pode, 2015). Almost all Li-ion battery is “deep cycle” implying that they can be completely charged and discharged.

3.7.3 Cycle Life

With 80% discharge rate, the typical life cycle of Li-ion cell varies from 500-1000 cycles (except for phosphate: 1000-2000) while it is 200-300 cycles for Lead-acid battery (Diouf & Pode, 2015). On the other hand, the cycle life of Vanadium redox is greater than 10,000 cycles with 100% DOD (depth of discharge). So, lithium-ion battery has altogether higher life cycle than a lead-acid battery.

3.7.4 Rate Execution

While figuring out what limit of a battery to use for a framework, a basic thought for a lead-acid battery is to what extent the framework will take to discharge. Along with shorter discharge period, we will get less capacity from a lead-acid cell. There are two distinct categories of lead-acid battery: flooded and sealed/valve regulated (SLA or VRLA). A 100Ah Li-ion cell will accomplish more than 98Ah within 30-minute discharge while 100Ah VRLA cell will just convey 80Ah in 4-hour time (Wanga, Adelmanna, & Reindla, 2012).

3.7.5 Frosty Weather Performance

In cold ambience, both lithium-ion and lead-acid battery lose capacity, but into the -20°C territory Li-ion loses altogether less capacity.

3.7.6 Ecological Impact & Recycling

Li-ion batteries are more environment friendly than lead-acid or vanadium but reusing of Li-ion cell are costlier than lead-acid batteries (Wanga, Adelmanna, & Reindla, 2012). It requires mining of lithium carbonate, aluminum, copper and iron metal. On the other hand, lead is extremely unsafe for a human being. More than 96% of lead-acid batteries in the USA are reused which has a huge effect on the natural condition.

3.7.7 Analysis of Cost

Generally, for the identical size, Li-ion battery is costlier than lead-acid. In our HOMER simulation, we can design the system in such way that we will get minimum COE (cost of energy).

The cost development of three types of batteries has been presented in table 3.3. Here we consider the hub height is 24 meters for wind turbine and operating temperature of the solar cell is 47°C. In the beginning, we put some values for capital cost, replacement cost and maintenance cost to get optimized results. Then HOMER simulates with these given input data and gives us the simulated results for each of the storage devices.

TABLE 3.3 COST ANALYSIS FOR BATTERIES

Input Parameters	Wind Turbine	PV Module	Converter	Li-ion	Lead-acid	Vanadium
Capital Cost ($)	2000	4615	420	30	200	5000$(Cell Stacks-kw),200$ (Electrolyte-kwh)
Replacement Cost ($)	1540	3692	350	28	150	1000$(Cell Stacks-kw),200$(Electrolyte-kwh)
O & M ($)	8	8	1	1	10	100
Lifetime(year)	20	25	15	8	6	15
Efficiency (%)	-	13	90	100%-20hr rate 99% at 4hr rate	100%-20hr rate 80% at 4hr rate	65-75%
Minimum SOC (%)	-	-	-	20	-	20
Nominal Voltage	-	-	-	3.7	2	50
Nominal Capacity(kwh)	-	-	-	1	1.03	-

From the following simulation results of cost (figure 56), we can see that Vanadium-ESS cell stack has the highest capital, replacement, and maintenance cost while lithium-ion has the minimum cost.

(a) (b) (c)

Figure 56: Cost summary of (a) 1 kW Li-ion [ASM] (b) 1 kW Lead-acid [ASM] (c) Generic Vanadium

3.7.8 Electricity Production & State of Charge (SOC)

From the HOMER simulation results based on wind and solar data, we can see that Li-ion battery has the highest electricity production per year which is 47,560 kWh/yr whether the amount is 47,329 kWh/yr and 47,330 kWh/yr for Lead-acid and Vanadium respectively.

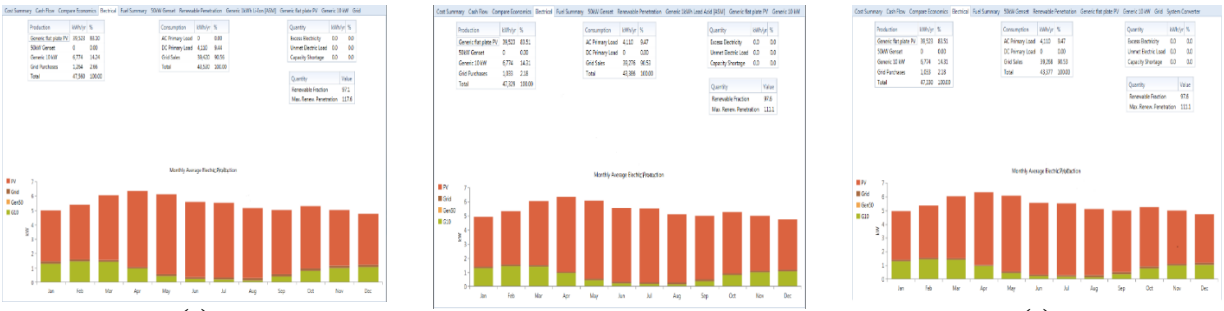

(a) (b) (c)

Figure 57: Monthly electric production for (a) Li-ion (b) Lead-acid (c) Generic Vanadium

On the other hand, Vanadium has almost 100% SOC while the value is 51% and 22.5% for lead-acid and lithium-ion respectively. Simply defined, state of charge (SOC) of a battery or cell is the percentage of its total energy capacity that is still available to discharge (Erdinc,

Vural, & Uzunoglu, A dynamic lithium-ion battery model considering the effects of temperature and capacity fading, 2009).

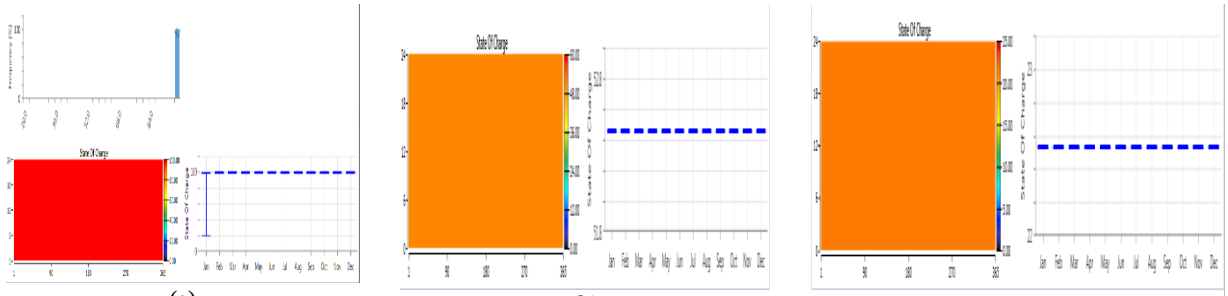

(a) (b) (c)

Figure 58: SOC of (a) Vanadium (100%) (b) Lead-acid (51%) (c) Li-ion (22.5%)

CHAPTER 4

RESULTS

4.1 Lithium-Ion Battery

4.1.1 Li-Ion Battery Aging Model

The ANN model for the proposed range of temperature and cycle as model inputs, with the corresponding values of eight outputs, is presented. Figure 59-66 gives the outputs of different parameters at different temperature (25℃ to 55℃) for ANN models.

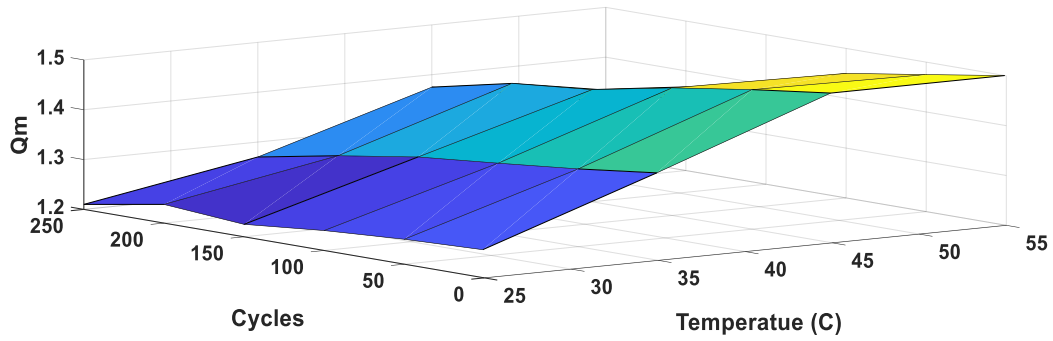

Figure 59: Maximum charge storage capacity (Q_m)

Figure 59 shows that Maximum charge storage capacity ($Q_{m)}$ gradually decreases with the increasing number of cycles. This is due to the degradation mechanisms of irreversible capacity loss are increased by temperature (Ning, 2003).

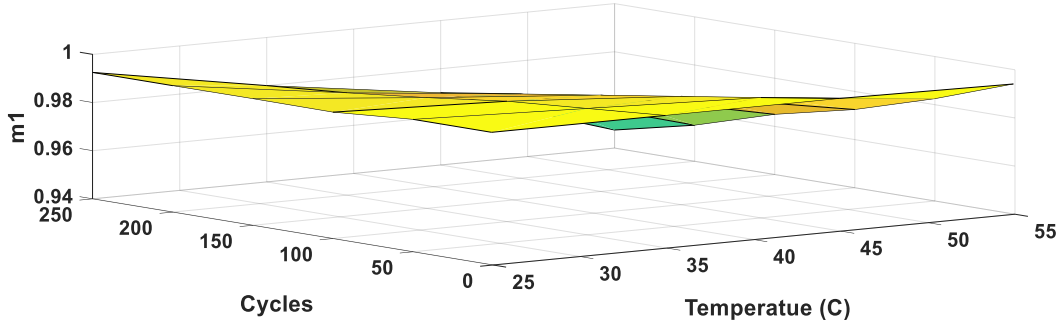

Figure 60: The aging of m1 of cobalt-oxide electrode

Figure 60 shows the degradation of m_1 of an LCO (lithium cobalt-oxide) electrode with cycling at different temperatures ranging from 25°C to 55°C. The degradation of m_1 is due to two mechanisms. One is the formation of the surface film and its subsequent modification on the electrode, and another one is the structural/phase changes of the electrode (Zhang D. e., 2000).

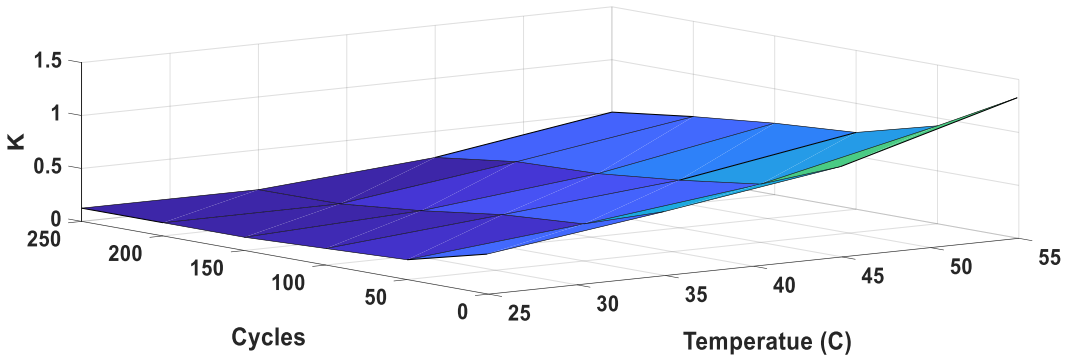

Figure 61: The aging of rate constant vs. temperature

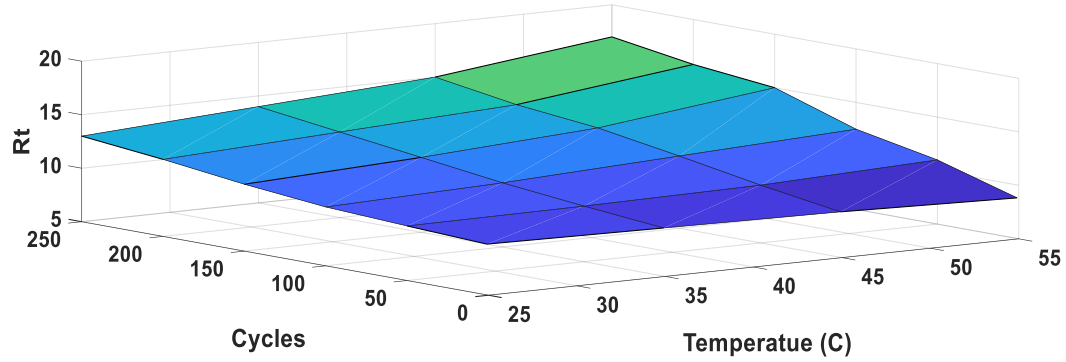

Figure 62: Total resistance of electrodes resistance and electrode/electrolyte resistance

Hence, both mechanisms result in a decrease in the charge transfer rate (K) with cycling. This charge transfer rate shows the rate of Li+ transport as it goes from electrode to electrolyte and from electrolyte to electrode (Winter, 2010). This two mechanisms will decrease the transport rate, and this is observed in figure 61. Both will also increase the electrode's impedance, and this is observed in figure 62.

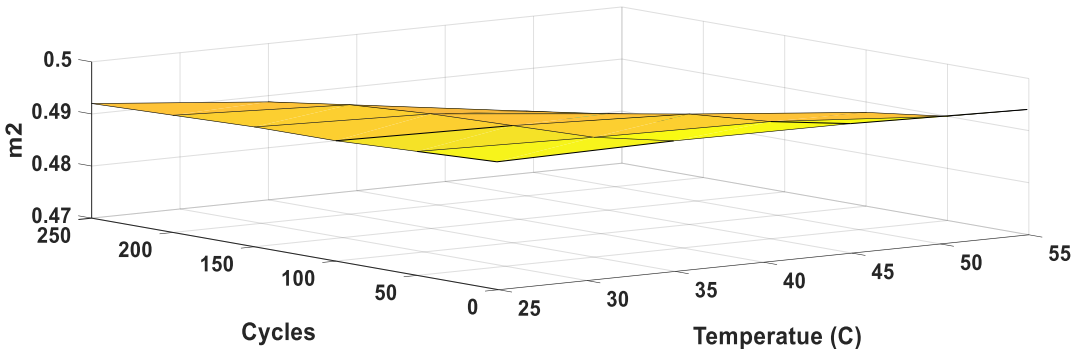

Figure 63: The aging of m2 of graphite electrode

Figure 63 shows the degradation of the m2 of the graphite electrode with different cycle number. The m2 in the ECBE (electrochemistry-based model) model describes the effectiveness of the graphite electrode for providing its stored Li-ions (L., T., Pecht, & Z, 2014). This degradation mainly due to the formation of the SEI (presence of surface film) and its growth on the surface of the graphite electrode.

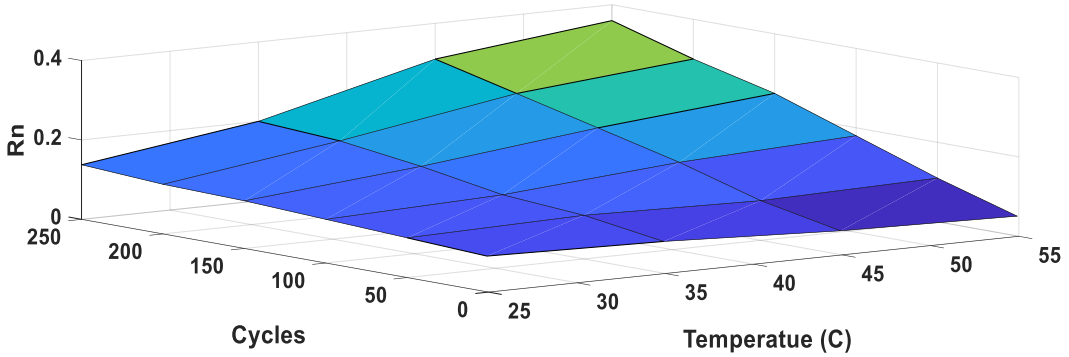

Figure 64: The aging of Warburg element resistance

Warburg element can be used to determine the aging of the electrolyte. This Warburg element models the electrolyte as a dielectric of a parallel plate capacitor with the two electrodes as the two plates of a capacitor. It designs the electrolyte system as a series of Rw and Cw where Rw is known as the resistance of the electrolyte and Cw is related to the capacitance of the equivalent parallel plate capacitor.

As temperature increases from 25°C to 55°C, the diffusivity of active Li-ions in the electrolyte Increases (Park, 2010) due to the increase in Qm (maximum charge storage capacity) as a result of the enhanced electrochemical reduction-oxidation (redox) at anode and cathode. As a result, a decrease in the resistance of the electrolyte is observed when the cell is initially cycled, as shown in figure 64.

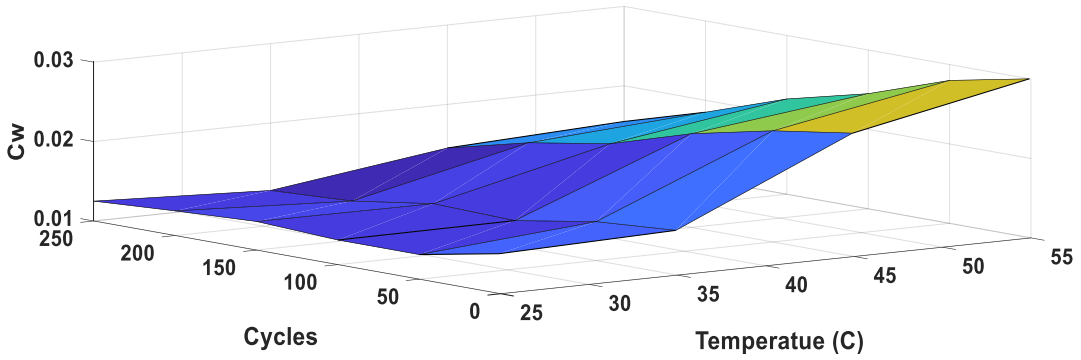

Figure 65: The aging of Warburg element capacitance

On the other hand, the Warburg element capacitance increases with temperature as shown in figure 65. This is due to the formation of SEI on the electrodes and separator that decrease the available surface of the active materials during cycling.

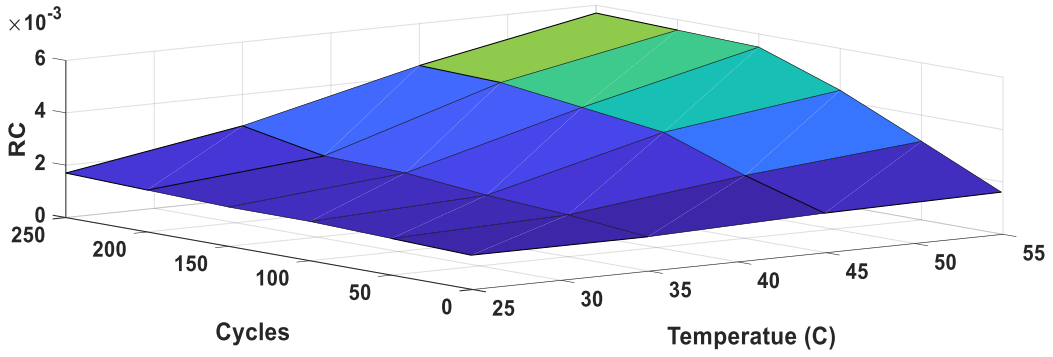

Figure 66: The aging of Warburg RC time constant

From figure 66, we can see that increasing the temperature will increase the rate of RC, and this indicates that the response to the change in current deliver from lithium-ion batteries will become slower at high temperature.

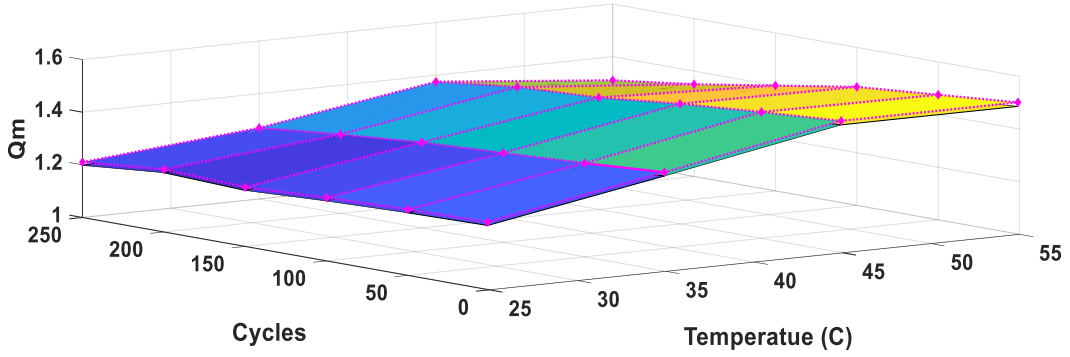

Figure 67: Comparison between training and output data of aging model

Figure 67 shows the comparison between training and output data. For the training data, regression accuracy is 99.912% while it is 99.995% for the output data.

4.1.2 Li-Ion Battery Thermal Model

The ANN model for the proposed range of time, ambient temperature, and voltage as model inputs, with the corresponding values of State of Charge (SOC) and Internal Temperature as outputs is presented. Finally, algebraic equations for the ANN model could be deduced. The proposed neural network unit is using the back propagation (BP) learning algorithm due to its benefits. The validity of this unit comes from the comparison between real values with corresponding from Neural Network obtained in MATLAB environment. The ANN training and testing data are extracted from Mathwork Model for lithium-ion Simulink model (M. & Dessaint, n.d.). Figure 68-70 gives the outputs of different parameters at different temperature for ANN models.

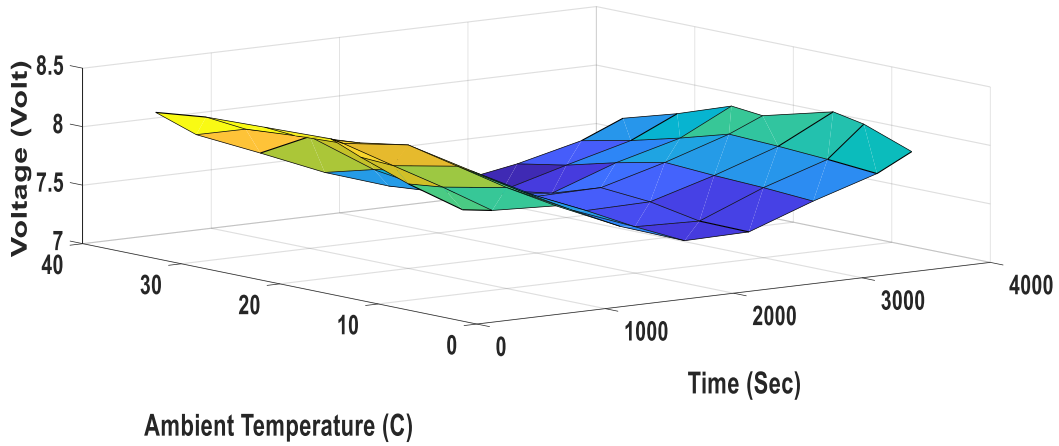

Figure 68: Output voltage in volts at different temperature

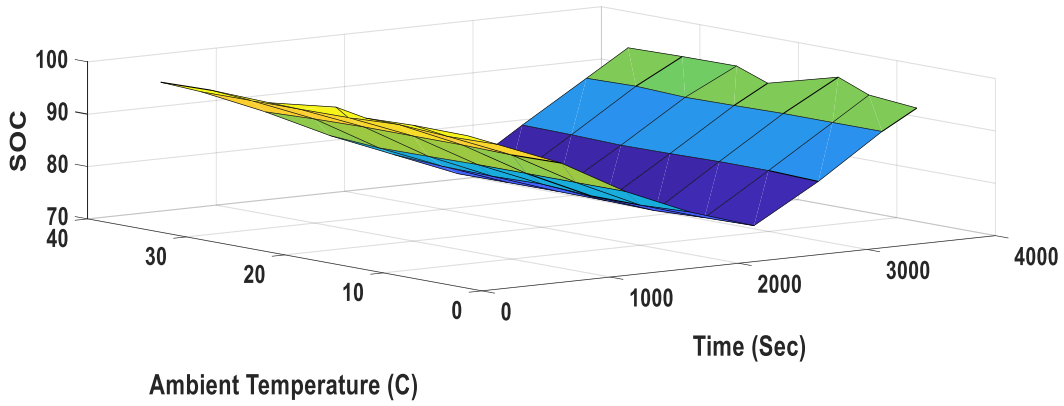

Figure 69: State of Charge (SOC) at different temperature

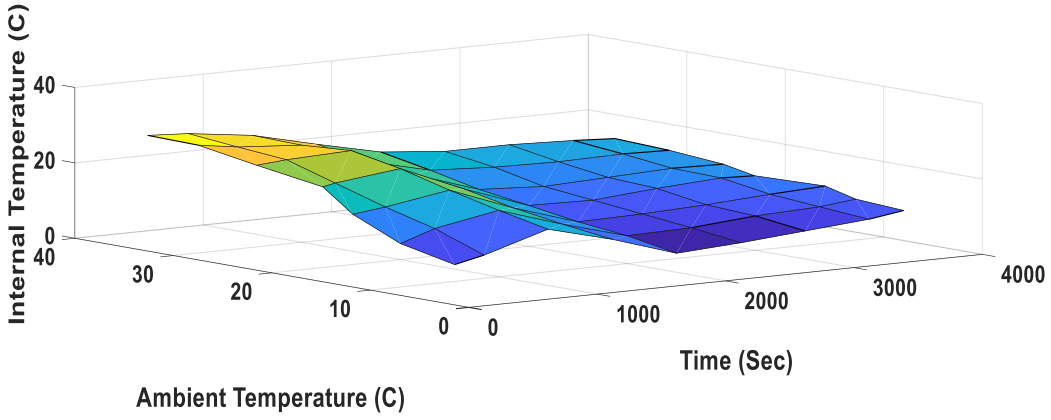

Figure 70: Ambient & Internal temperature in Celsius

From the above figures, it is observed that the temperature dependent battery model performs close to reality. Due to the increase in ambient temperature from 5 to 35ºC, battery SOC and internal temperature also increase. As the cell/internal temperature increases/decreases due to charge (or discharge) heat losses and ambient temperature variations, the output voltage and capacity also increase/decrease.

4.2 Lead-Acid Battery Thermal Model

The ANN model for the proposed range of time, ambient temperature and voltage as model inputs, with the corresponding values of State of Charge (SOC), Depth of Charging (DOC), Current, Internal Temperature and Heat Flow as outputs is presented. Finally, algebraic equations for the ANN model could be deduced. The proposed neural network unit for lead-acid battery is also using the back propagation (BP) learning algorithm due to its advantages.

Figure 71-75 gives the outputs of different parameters at different temperature for ANN models.

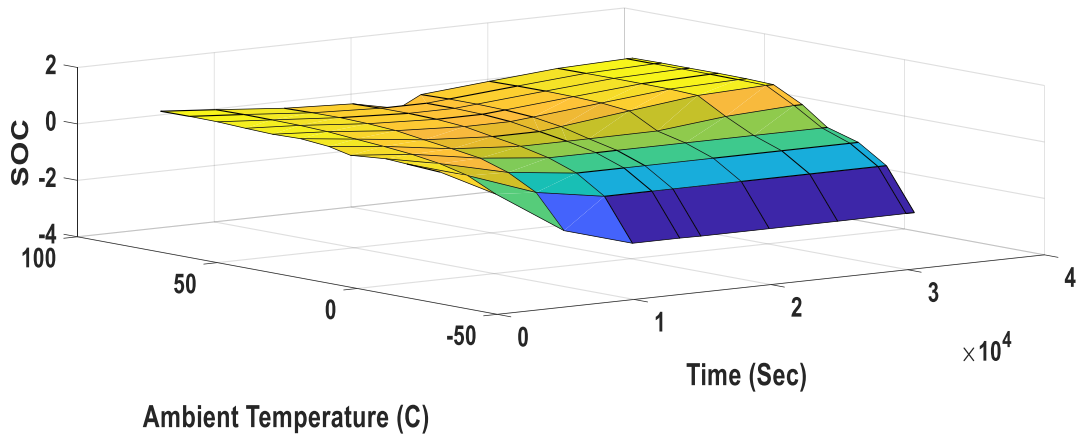

Figure 71: State of Charge (SOC) at different temperature range

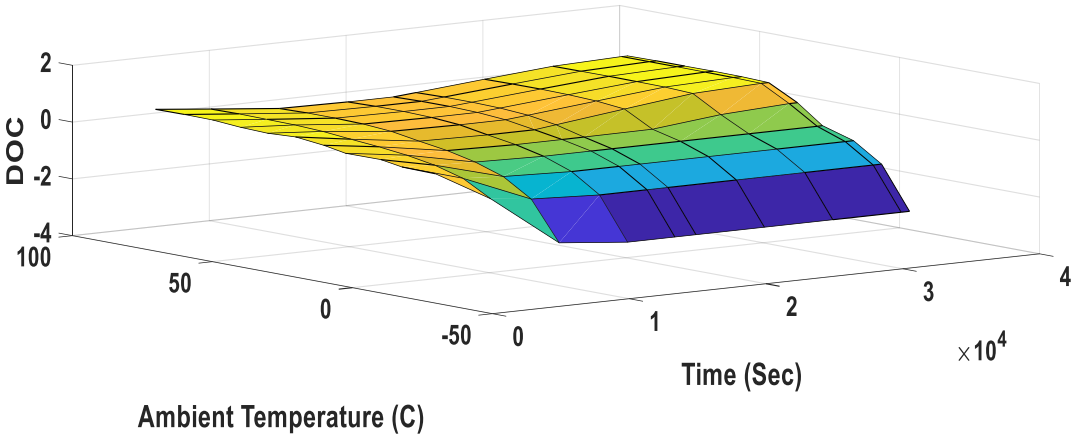

Figure 72: Depth of Charge (DOC) at different temperature range

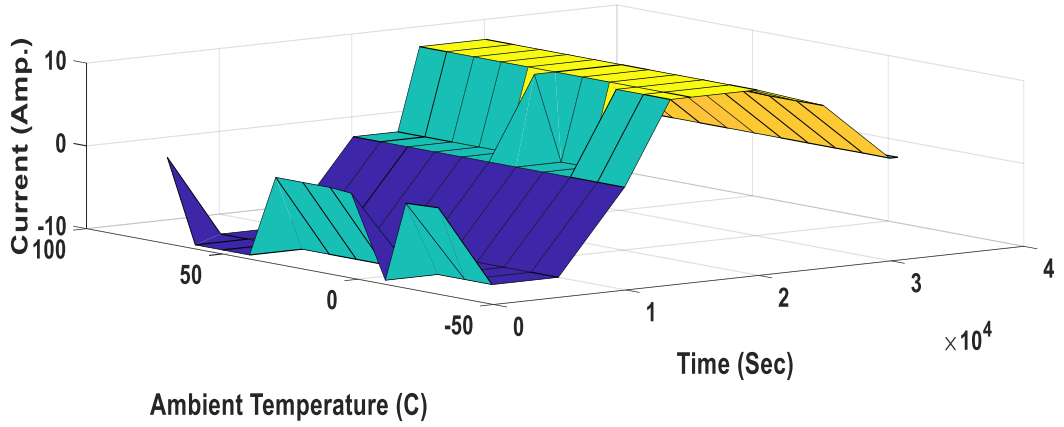

Figure 73: Charging/Load current in ampere at different temperature range

In this simulation process, at first, the battery is discharged at a constant current of 10A. The battery is then recharged at a constant 10A back to the initial condition of charge.

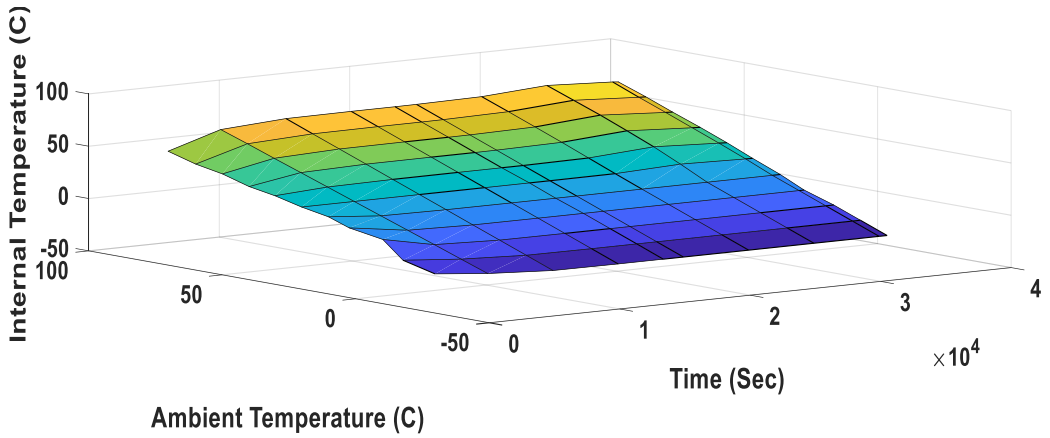

Figure 74: Internal temperature in Celsius

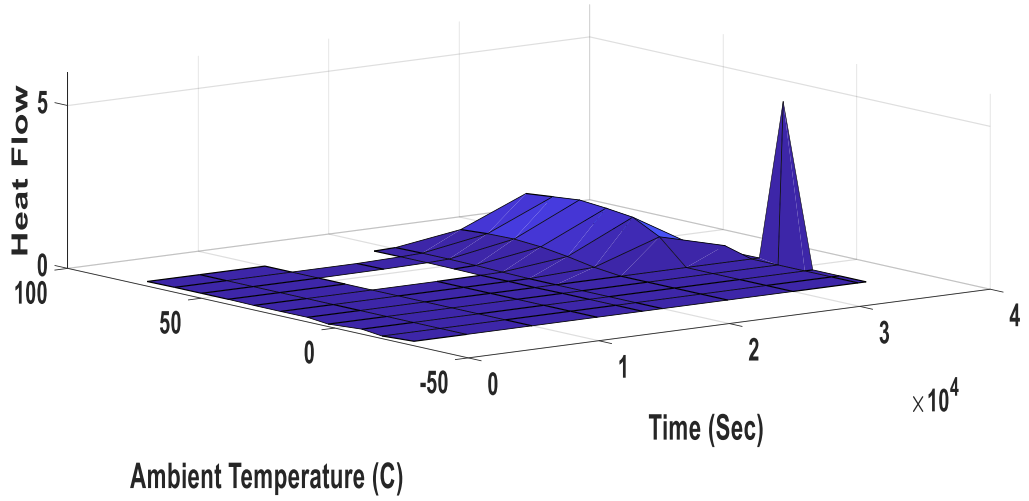

Figure 75: Heat flow in watts at different temperature range

From the above figures, it is clear that with the increase of ambient temperature from -5 to 75ºC, battery SOC & DOC, internal temperature, heat flow, also increases.

4.3 Output from HOMER

4.3.1 Optimization Results

In this study, we have considered residential load. Assuming that, the lifetime of the whole project is 25 years. Based on different optimization results on various case we have created a comparison table for these storage devices.

Table 4.1 OPTIMIZATION OUTPUTS FOR DIFFERENT BATTERIES

No	Simulation Type	Li-ion COE ($/kWh)	Lead-acid COE ($/kWh)	Vanadium COE ($/kWh)
1	Solar & wind with grid	0.0620	0.0731	0.0599
2	Solar & wind without grid	1.11	1.23	2.4
3	Solar with grid	0.0771	0.0759	0.353
4	Solar without grid	1.06	1.23	12.96
5	Wind with grid	0.0499	0.0386	0.0281
6	Wind without grid	0.238	10.40	17.24

From the above table we can clearly see that in case of solar & wind with the grid, the minimum COE (cost of energy) from the result is 0.0620$, 0.0731$ and 0.0599$ respectively. In this scenario, the percentage of renewable energy contribution is 97%, 98%, and 98% respectively for Li-ion, Lead-acid and Vanadium battery. For other types of simulation, the COE is quite high except wind with grid simulation result. As the wind speed is good enough for Statesboro, GA we get another minimum COE which is 0.0499$, 0.0386$ and 0.0281$ respectively. However, without grid connection for lead-acid battery COE is high enough which is 10.40$.

In the proposed grid connected model, an optimum number of renewable energy sources is activated and supplies electricity to the load. From figure 76 & 77, it can be clearly seen that for Li-ion battery, the off-grid power system for the same load is more expensive (1.11$/kWh) than grid-connected system (0.0620$/kWh) which is true for the other mentioned storage devices.

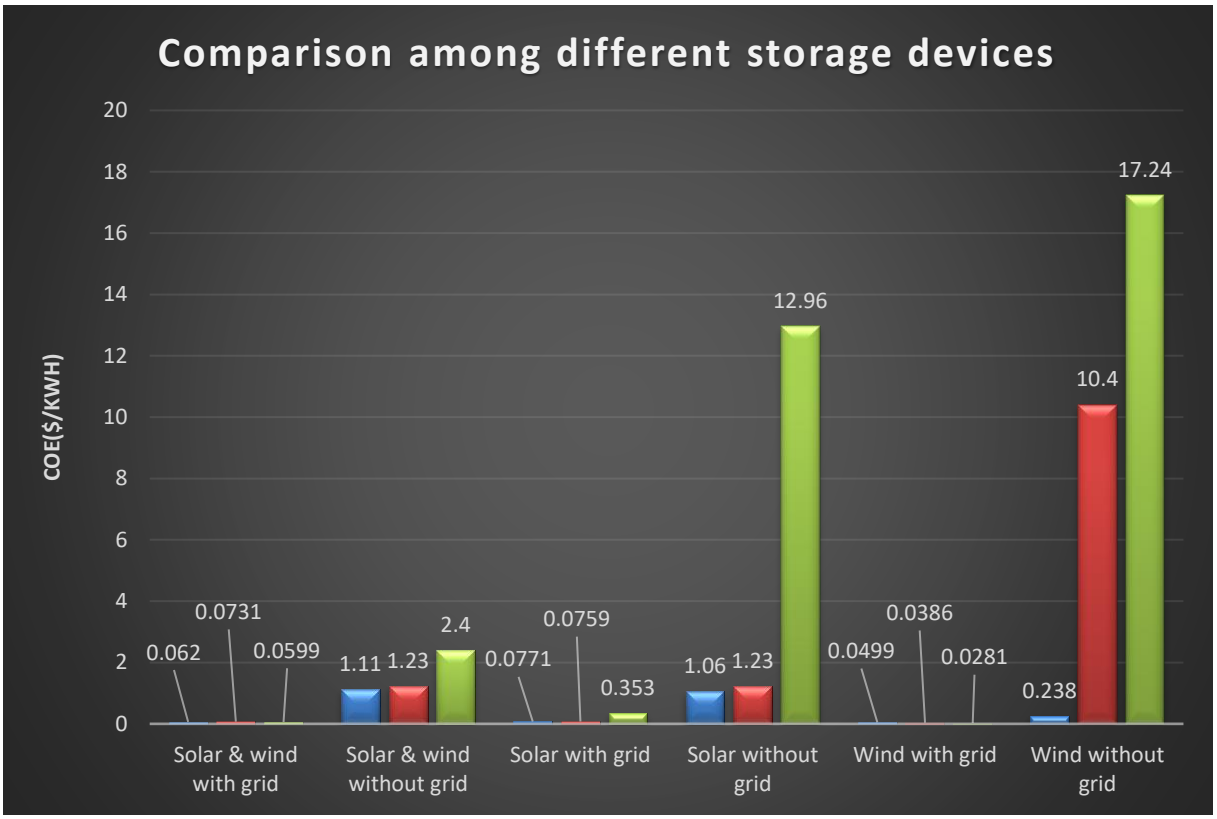

Figure 76: Comparison among three different storage devices

Based on table 4.1 we have created a comparison chart among those storage devices which is shown in figure 76. In case of solar without the grid simulation, the COE is 12.96 $/kWh for the vanadium battery. On the other hand, for wind without grid simulation, another highest COE is observed which is 10.4 $/kWh and 17.24 $/kWh respectively for lead-acid and vanadium battery. Figure 77-80 shows the optimized outputs for different storage devices with and without grid connection.

Architecture														Cost				System
						PV (kW)	PV-MPPT (kW)	G10	Gen50 (kW)	LI ASM	Grid (kW)	Converter (kW)	Dispatch	COE ($)	NPC ($)	Operating cost ($)	Initial capital ($)	Ren Frac (%)
						25.0	25.0	1	100	20	999,999	28.0	CC	$0.0620	$34,868	-$1,230	$50,770	97
						25.0	25.0		100	20	999,999	28.0	CC	$0.0771	$37,495	-$872.18	$48,770	94

Figure 77: Screenshot of optimized results (Li-ion/grid connected)

Architecture												Cost				System
					PV (kW)	PV-MPPT (kW)	G10	Gen50 (kW)	LI ASM	Converter (kW)	Dispatch	COE ($)	NPC ($)	Operating cost ($)	Initial capital ($)	Ren Frac (%)
					25.0	25.0		100	20	28.0	CC	$1.06	$56,397	$589.96	$48,770	100
					25.0	25.0	1	100	20	28.0	CC	$1.11	$58,714	$614.54	$50,770	100

Figure 78: Screenshot of optimized results (Li-ion/without grid)

Architecture														Cost			System
						PV (kW)	PV-MPPT (kW)	G10	Gen50 (kW)	LA ASM	Grid (kW)	Converter (kW)	Dispatch	COE ($)	NPC ($)	Operating cost ($)	Initial capital ($)	Ren Frac (%)
						25.0	25.0	1	100	20	999,999	28.0	CC	$0.0731	$40,986	-$1,020	$54,170	98
						25.0	25.0		100	20	999,999	28.0	CC	$0.0901	$43,561	-$665.96	$52,170	95

Figure 79: Screenshot of optimized results (Lead-acid/grid connected)

Architecture															Cost			System
						PV (kW)	PV-MPPT (kW)	G10	Gen50 (kW)	V-ESS (kW)	V-ESS (kWh)	Grid (kW)	Converter (kW)	Dispatch	COE ($)	NPC ($)	Operating cost ($)	Initial capital ($)	Ren Frac (%)
						25.0	25.0	1	100			999,999	28.0	CC	$0.0599	$33,617	-$1,280	$50,170	98
						25.0	25.0		100			999,999	28.0	CC	$0.0749	$36,192	-$926.54	$48,170	95

Figure 80: Screenshot of optimized results (Vanadium/grid connected)

The simulation results show that, a grid-connected hybrid power system with various storage devices which includes solar and wind is more cost-effective than without grid-connected hybrid power system for the same residential load. If we want to supply power to the grid, then Li-ion battery would be an excellent choice. Moreover, if we go with an only wind turbine, then Vanadium would be more cost-effective battery among these. In our proposed system the COE for lithium-ion battery with grid connection is 0.0620/0.0731/0.0599$/kWh while the average residential electricity rate in Statesboro is 0.116$/kWh (Electricity Local, n.d.). So, our designed HOMER model is more cost-efficient.

CHAPTER 5

CONCLUSION

5.1 Summary of Present Work

In this study, a thermal model of lithium-ion and a lead-acid battery along with an aging model of lithium-ion battery is designed with the help of Artificial Neural Network (ANN). Then we used these storage devices to simulate using HOMER to find out minimum cost of energy for electricity production. In a nutshell, major findings are listed below:

- Li-ion battery aging model is created with the help of ANN.
- Effect of temperature on the aging rate is depicted with the help of 3D figure for various characteristics like maximum charge storage capacity, aging of graphite electrode, aging of Warburg element capacitance/resistance/RC time constant, etc.
- An accurate Artificial Neural Network model is developed for the thermal model of lithium-ion and lead-acid battery using MATLAB.
- Several types of model parameters like SOC, DOC, load current, heat flow, etc. are well described in the form of a 3D figure as the training data for ANN models.
- Then ANN technique models are adopted to generalize the process for modeling and characteristics estimation for the whole capacity rates range due to its advantages.
- These ANN models are created with suitable numbers of layers and neurons, trained, simulated, checked, and their algebraic equations concluded accurately with excellent regression constant.
- A wind-solar hybrid power system is designed for Statesboro, Georgia using HOMER.
- Both off-grid and on-grid system designed and optimized for comparison purposes.

- The cost analysis is performed utilizing HOMER software based on solar irradiance, wind speed, and load profile.
- Economic comparison of lithium-ion, lead-acid and vanadium is presented. Cost correlation of these batteries is also discussed via net present cost (NPC).
- The cost comparison is done using HOMER based on solar and wind data for Statesboro.

5.2 Future Work

Although lots of research work has been done and continuously going to storage device application, there are still some opportunities to accelerate the revolution in this field. Here some future works recommended below

- Still, there is scope to study about the comprehensive effects of temperature on the cyclic aging rate of lithium-ion batteries.
- The lithium-ion battery usability can be expanded with maximum allowable temperature range.
- ANN can be used for predictive controlling to enhance the overall performance of a battery.
- Application for partial discharge (PD) recognition, ANN could be a solution.
- Artificial Intelligence like PSO (Particle Swarm Optimization) or Genetic Algorithm can be done using ANN to drive batteries at an enhanced performance. Then Fuzzy Logic controller can be implemented.
- HOMER simulation model can be implemented practically in a remote locality where grid connection is not available.
- The proposed HOMER model could be a solution for producing electricity at lower cost for any developing country.

REFERENCES

(n.d.). Retrieved from Encyclopaedia britannica: https://www.britannica.com/science/renewable-energy

(EIA), U. D. (April 2015). *Annual Energy Outlook.*

(EIA), U. D. (April, 2015). *Annual Energy Outlook 2015.*

(2010, July). Retrieved from Department of Energy and Climate Change: http://www.decc.gov.uk/en/content/cms/meeting_energy/aes/aes.aspx.

(2012, June). Retrieved from BP Statistical Review of World Energy.: http://www.bp.com/sectionbodycopy.do?categoryId=7500&contentId=7068481.

(2017). Retrieved from Global Energy Statistical Yearbook: https://yearbook.enerdata.net/renewables/renewable-in-electricity-production-share.html

Al Shamisi, M. H., Assi, A. H., & Hejase, H. A. (2011). *Using MATLAB to Develop ANN Models for Predicting Global Solar Radiation in Al Ain City – UAE.* United Arab Emirates.

Albright, G., edie, J., & Al-Hallaj, S. (2012). *A Comparison of Lead-Acid to Lithium-ion in Stationary Storage Applications.* ALLCell Technologies LLC.

(April 2015). *Annual Energy Outlook.* U.S. department of Energy (DoE) / Energy Information Administration (EIA).

Bernardi, D., Pawlikowski, E., & Newman, J. (1985). *A general energy balance for battery systems.*

Bernardi, D., Pawlikowski, E., & Newman, J. (1985). *A general energy balance for battery systems.* J. Electrochem. Soc.

Boroyevich, D., Cvetkovic, I., Burgos, R., & Dong, D. (Sept 2013). Intergrid: A Future Electronic Energy Network. *IEEE Joutnal of Emerging and Selected Topics in Power Electronics*, 127-138.

Boroyevich, D., Cvetkovic, I., Burgos, R., & Dong, D. (Sept. 2013). Intergrid: A Future Electronic Energy Network. *IEE Journal of Emerging and Selected Topics in Power Electronics*, 127.

Broussely, M., Biensan, P., Bonhomme, F., Blanchard, P., Herreyre, S., Nechev, K., & Staniewicz, R. (2005). Main aging mechanisms in Li ion batteries. *Journal of Power Sources*, 90-96.

Chen, M., & Mora, G. (2006). Accurate electrical battery model capable of predicting runtime and I-V performance. *IEEE Transactions on Energy Conversion*, (pp. 504-511).

Chen, M., & Rincon-Mora, G. A. (05 June 2006). Accurate electrical battery model capable of predicting runtime and I-V performance. *IEEE TRANSACTIONS ON ENERGY CONVERSION*, (pp. 504-511).

Chen, S., SMIEEE, Tseng, K., & Choi, S. (May 2009). Modeling of Lithium-Ion Battery for Energy Storage System Simulation. *IEEE Power & Energy Society (PES).* Wuhan University.

Clanku, & Martin, B. (September, 2012). *A dynamic battery model considering the effects of the temperature and capacity fading.*

Corporation, A. (n.d.). Simulation System SIMPLORER VHDL-AMS Tutorial.

Crompton, T. (2000). *Battery Reference Book.* Newnes, Oxford.

Cvetkovic, I. (July,2010). *Modeling, Analysis and Design of Renewable Energy Nanogrid Systems.* Blacksburg, Virginia.

Cvetkovic, I., Thacker, T., Dong, D., Francis, G., Podosinov, V., Boroyevich, D., . . . Lesko, J. (2009). Future home uninterruptible renewable energy system with vehicle-to-grid technology. *Energy Conversion Congress and Exposition, ECCE* (pp. 2675-2681). IEEE.

Diouf, B., & Pode, R. (2015). Potential of lithium-ion batteries in renewable energy. Renewable Energy.

Doerffel, D., & Sharkh, S. A. (April 2006). A Critical Review of Using the Peukert equation for Determining the Remaining Capacity of Lead-acid and Lithium-ion Batteries. *Journal of Power Systems*, 395-400.

Dunn, B., Kamath, H., & Tarascon, J. (2011). Electrical energy storage for the grid: A battery of choices. 928-935.

Dunn, B., Kamath, H., & Tarascon, J. (2011). Electrical energy storage for the grid: A battery of choices. 928-935.

Duong, T. (2013). *DESIGN, MANAGEMENT AND CONTROL OF ENERGY STORAGE DC NANO-GRID.* Singapore.

El Shahat, A. (2014). Neural Network Storage Unit Parameters Modeling. *International Journal of Industrial Electronics and Drives*, 249-274.

El Shahat, A., Haddad, R. J., & Kalaani, Y. (2015). An Artificial Neural Network Model for Wind Energy Estimation. *IEEE SoutheastCon.* Florida.

Electricity Local. (n.d.). Retrieved from www.electricitylocal.com: http://www.electricitylocal.com/states/georgia/statesboro/

El-Shahat, A. (2014). *Artificial Neural Network (ANN): Smart & Energy Systems Applications.* Germany: Scholar Press Publishing.

Enclyclopaedia Britannica. (n.d.). Retrieved from https://www.britannica.com/science/renewable-energy

Erdinc, O., Vural, B., & Uzunoglu, M. (2009). A dynamic lithium-ion battery model considering the effects of temperature and capacity fading. *Clean Electrical Power, 2009 International Conference*, (pp. 383-386).

Erdinc, O., Vural, B., & Uzunoglu, M. (2009). A dynamic lithium-ion battery model considering the effects of temperature and capacity fading. *International conference on Clean Electrical Power*, (pp. 383-386). Capri.

Eriksson, K. (Nov 2011). Operational experience of HVDC Light™. *Seventh International Conference on AC and DC Transmission,*, (pp. 205-210).

et, I. d. (2017). *Artificial Neural Networks.* Switzerland: Springer International Publishing.

Gao, L., Liu, S., & Dougal, R. (2002). Dynamic Lithium-Ion Battery Model for System Simulation. *IEEE Transactions on Components and Packaging Technologies*, (pp. 495-505).

Gao, L., Liu, S., & Dougal, R. A. (2002). Dynamic Lithium-Ion Battery Model for System simulation. *IEEE Trans. Comp. Package. Technology*, (pp. 495-505).

Gao, L., Liu, S., & Dougal, R. A. (September 2002). Dynamic Lithium-Ion Battery Model for System simulation. *IEEE Trans. Comp. Package. Technology, ,* (pp. 495-505).

Giraud, F., & Salameh, Z. M. (2001). Steady-state performance of a grid-connected rooftop hybrid wind-photovoltaic power system with battery storage. *IEEE transactions on energy conversion*, (pp. 16(1), 1-7).

Givler, T., & Lilienthal, P. (2005). *HOMER software, NREL's micropower optimization model, to explore the role of gensets in small solar power systems.* Golden, Colorado.

Groot, J. (2014). *State-of-Health Estimation of Li-ion Batteries: Ageing Models.* Sweden.

Guarnieri, M., Mattavelli, P., Petrone, G., & Spagnuolo, G. (Dec 2016). Vanadium Redox Flow Batteries: Potentials and Challenges of an Emerging Storage Technology. *IEEE Industrial Electronics Magazine*, (pp. 20-31).

Jackey, A. R. (2007). *A Simple, Effective Lead-Acid Battery Battery Modeling Process for Electrical System Component Selection.*

Jackey, R. A. (n.d.). *A Simple, Effective Lead-Acid Battery Modeling Process for Electrical System Component Selection.* 2007: Mathworks.

Johnson, V., Pesaran, A., & Sack, T. (2002). *Temperature dependent battery models for high-power lithium-ion batteries.*

Johnson, V., Pesaran, A., & Sack, T. (2002). *Temperaturedependent battery models for high-power lithium-ion batteries.*

Johnson, V., Pesaran, A., & Sack, T. (2002). *Temperaturedependent battery models for high-power lithium-ion batteries.*

Kennedy, B., Patterson, D., & Camilleri, S. (2000). Use of lithium-ion batteries. *Journal of Power Sources*, 156-162.

Konrad, T., Loria, W., Miller, T., & Yamasaki, M. (May 5, 2014). *DC Microgrid.*

L., F., T., C. M., Pecht, M., & Z, J. (2014). The effect of temperature on the electrochemistry in Lithium-ion batteries. *3rd International Symposium on Next-Generation Electronics.* Taoyuan, Taiwan,: IEEE Computer Society.

Lagorse, J., Simoes, M. G., Miraoui, A., & Costerg, P. (2008). Energy cost analysis of a solar-hydrogen hybrid energy system for stand-alone application. *International journal of hydrogen energy*, 2871-2879.

Lambert, T., Gilman, P., & Lilienthal, P. (2006). *MICROPOWER SYSTEM MODELING WITH HOMER.* Mistaya Engineering Inc.

Leng, F. e. (2015). *Effect of Temperature on the Aging rate of Li-ion Battery Operating above Room Temperature.* Scientific Reports.

Leng, F. e. (2015). Effect of Temperature on the Aging rate of Li-Ion Battery Operating above Room Temperature. *Scientific Reports*.

Leng, F., Tan, C. M., Rachid, Y., & Le, M. D. (2014). A practical framework of electrical based online state-of-charge estimation of lithium ion batteries. *Journal of Power Sources*, 423-430.

lilienthal, P., Gilman, P., & Lambert, T. (2005). *HOMER micropower optimization model.* Department of Energy, United States.

Loh, P. C., Chai, Y. K., & Blaabjerg, F. (May 2013). Autonomous operation of Hybrid Microgrid with AC and DC subgrids. *IEEE Transactions on Power Electronics*, (pp. 2214-2223).

M., N. S., & Dessaint, L.-A. (n.d.). *MathWorks*.

Narula, A. (2014). *Modeling of Ageing of Lithium-Ion Battery at Low Temperatures.* Goteborg, Sweden.

Ning, G. H. (2003). Capacity fade study of lithium-ion batteries cycled at high discharge rates. *J. Power Sources*, 160-169.

Park, M. Z. (2010). A review of conduction phenomena in Li-ion batteries. *J. Power Sources*, 7904–7929.

Ramadass, P., Haran, B., White, R., & Popov, B. N. (2003). Mathematical modeling of the capacity fade of Li-ion cells. *Journal of Power Sources*, 230-240.

Reno, M. J., Hansen, C. W., & Stein, J. S. (2012). *Global horizontal irradiance clear sky models: implementation and analysis.* SANDIA report SAND2012-2389.

S., S., C., R., & A., E. (April, 2004). Electrical Modeling of Renewable Energy. *Journal of Power Electronics*.

S., Williamson; C., Rimmalapudi; A., Emadi. (April, 2004). *Journal of Power Electronics*.

Salameh, Z. M., & Davis, A. J. (2003). Case study of a residential-scale hybrid renewable energy power system in an urban setting. *Power Engineering Society General Meeting* (p. 2322). IEEE.

Sarkar, J., & Khule, S. (2016). A Study of MPPT Schemes in PMSG Based Wind Turbine System. *ICEEOT Conference.* India.

Silva, D., Spatti, H., Flauzino, A., & Liboni, L. (2016). *Artificial Neural Networks.*

Smith, K. (2006). *Electrochemical Modeling, Estimation and Control of Lithium-ion Batteries.* Retrieved from http://www.posterus.sk/?p=13560&output=pdf

Spotnitz, R. (2003). Simulation of capacity fade in lithium-ion batteries. *Journal of Power Souces*, 72-80.

Stan, A., Swierczynski, M., Stroe, D., Teodorescu, R., & Andreasen, S. J. (22-24 May 2014). Lithium ion battery chemistries from renewable energy storage to automotive and back-up power applications — An overview. *Optimization of Electrical and Electronic Equipment (OPTIM)*, (pp. 713-720).

Stan, A., Swierczynski, M., Teodorescu, R., & Andreasen, S. (22-24 May 2014). Lithium ion battery chemistries from renewable energy storage to automotive and back-up power applications — An overview. *Optimization of Electrical and Electronic Equipment (OPTIM)*, (pp. 713-720).

Stroe, D. (2015). Degradation Behaviour of Lithium-Ion Batteries based on Field Measured Frequency Regulation Mission Profile. *2015 IEEE Energy Conversion Congress and Exposition (ECCE)*, (pp. 14-21). Montreal, QC.

Stroe, D., M., S., Stan, A., Teodorescu, R., & Andreasen, S.-J. (Nov.-Dec.2014). Accelerated Lifetime Testing Methodology for Lifetime Estimation of Lithium-Ion Batteries Used in Augmented Wind Power Plants. *Industry Applications, IEEE Transactions* (pp. 4006-4017). IEEE.

Stroe, D., Swierczynski, M., Stan, A., Teodorescu, R., & Andreasen, S.-J. (Nov.-Dec.2014). Accelerated Lifetime Testing Methodology for Lifetime Estimation of Lithium-Ion Batteries Used in Augmented Wind Power Plants. *Industry Applications, IEEE Transactions*, (pp. 4006-4017).

Stroe, D.-I. (2014). *Lifetime Models for Lithium-ion Batteries used in Virtual Power Plant Applications.* PhD Thesis, Aalborg University.

Stroe, D.-I. (2015). Degradation Behaviour of Lithium-Ion Batteries based on Field Measured Frequency Regulation Mission Profile. *2015 IEEE Energy Conversion Congress and Exposition (ECCE)*, (pp. 14-21). Montreal, QC.

Stroe, D.-I., Knap, V., Swierczynski, M., Stroe, A.-I., & Teodorescu, R. (11 October 2016). Operation of Grid-Connected Lithium-Ion Battery Energy Storage System for Primary Frequency Regulation: A Battery Lifetime Perspective. *IEEE Transactions on Industry Applications*, (pp. 1-1).

Sureshkumar, U., Manoharan, P. S., & Ramalakshmi, P. S. (2012). Economic cost analysis of hybrid renewable enrgy system using HOMER. *In Advances in Engineering, Science and Management (ICAESM), International Conference on IEEE*, (pp. 94-99).

Swierczynski, M., Stroe, D., Stan, A., Teodorescu, R., & Sauer, D. (Jan. 2014). Selection and Performance-Degradation Modeling of LiMO2/Li4Ti5O12 and LiFePO4/C Battery Cells as Suitable Energy Storage Systems for Grid Integration With Wind Power Plants: An Example for the Primary Frequency Regulation Service. *Sustainable Energy, IEEE Transactions*, (pp. 90-101).

Timmermans, J.-M., Nikolian, A., Hoog, J. D., & Gopalakrishnan, R. (Sep 2016). Batteries 2020 – Lithium - ion battery first and second life ageing, validated battery models, lifetime modelling and ageing assessment of thermal parameters. *EPE'16 - ECCE: 18th European Conference on Power Electronics and Applications*, (p. 23).

Tremblay, O., Dessaint, L., & Dekkiche, A. (2007). A Generic Battery Model for the Dynamic Simulation of Hybrid Electric Vehicles. *Vehicle Power and Propulsion Conference.* Arlington/Texas: IEEE.

Tremblay, O., Dessaint, L., & Dekkiche, A.-I. (2007). A Generic Battery Model for the Dynamic Simulation of Hybrid Electric Vehicles. *Vehicle Power and Propulsion Conference.* Arlington, TX: IEEE.

Twidell, J., & Weir, T. (2006). *Renewable Energy Resources.* New york.

Tymvios, F., Michaelides, S., & Skouteli, C. (2008). *Estimation of Surface Solar Radiation with Artificial Neural Networks.* Germany.

U., S., P. S., M., & A. P. S., R. (2012). Economic Cost Analysis of hybrid renewable enrgy system using HOMER. *In Advance In Engineering, Science and Management (ICAESM)* (pp. 94-99). IEEE.

Vetter, J., Novak, P., Wagner, M., Veit, C., Moller, K.-C., Besenhard, J., . . . Vogler, C. (March, 2005). Ageing mechanism in li-ion batteries. *Journal of Power Sources*, 269-281.

Wanga, X., Adelmanna, P., & Reindla, T. (2012). Use of LiFePO4 batteries in Stand-Alone solar system. Energy Procedia 25.

Williamson, S., C, R., & A., E. (April 2004). Electrical Modeling of Renewable Energy Sources and Energy Storage Devices.

Winter, M. e. (2010). *Electrolytes, SEI and Charge Discharge Kenetics of Li-ion Batteries.*

Wright, S. D., Rogers, A. L., Manwell, J. F., & Ellis, A. (Jun 2002). Transmission options for offshore wind farms in the United States. Portland: Proc. AWEA Annual Conference, Portland.

Xing, Y., Ma, E. W., Tsui, K. L., & Pecht, M. (2011). *Battery Management Systems in Electric and Hybrid Vehicles.*

Ya azaki, T., Sakurai, K., & Muramoto, K. (1998). Estimation of the residual capacity of sealed lead-acid batteries by neural network. *INTELEC-Twentieth International Telecommunications Energy Conference* , (pp. 210-214). San Francisco, CA.

Zhang, D. e. (2000). Studies on capacity fade of lithium-ion batteries. *J. Power Sources*, 122-129.

Zhang, W. (May, 2015). *Energy Management System in DC Future Home.* Blacksburg: Virginia.

Zhang, W., Lee, F. C., & Huang, P. Y. (2014). Energy management system control and experiment for future home . *IEEE Energy Conversion Congress and Exposition (ECCE)*, (pp. 3317-3324). Pittsburgh, PA.